

RESEARCH ARTICLE

10.1029/2018JC013934

Origin, Transformation, and Fate: The Three-Dimensional Biological Pump in the California Current System

M. Frischknecht¹ , M. Münnich¹ , and N. Gruber¹ ¹Environmental Physics, Institute of Biogeochemistry and Pollutant Dynamics, ETH Zürich, Zürich, Switzerland

Key Points:

- The origin and fate of nutrients supporting nearshore production along central California are strongly separated in space and time
- Trajectories of central California coastal upwelling suggest a 3-D view of the biological pump that decouples carbon export from production
- Offshore export of carbon and nutrients support a large fraction of open ocean production and export downstream of coastal upwelling systems

Supporting Information:

- Supporting Information S1

Correspondence to:

M. Frischknecht,
martin.frischknecht@usys.ethz.ch

Citation:

Frischknecht, M., Münnich, M., & Gruber, N. (2018). Origin, transformation, and fate: The three-dimensional biological pump in the California Current System. *Journal of Geophysical Research: Oceans*, 123. <https://doi.org/10.1029/2018JC013934>

Received 22 FEB 2018

Accepted 4 OCT 2018

Accepted article online 11 OCT 2018

Abstract While the Ekman drift as the cause for the high productivity of the California Current System was unraveled more than a century ago, it is less clear where the nutrients within the upwelling waters are coming from, and what the fate of the produced organic matter is. Here we address these questions using a high-resolution simulation with a regional coupled physical/biogeochemical/ecological model within a Pacific Ocean setup. Our results, emerging from both Eulerian and Lagrangian analyses, reveal that prior to coastal production, inorganic nutrients get transported laterally over thousands of kilometers toward central California. More than 80% of the nutrients originate from central offshore or southern alongshore locations. About half of it is supplied by the California Undercurrent alone, underscoring its importance in sustaining the high coastal productivity. Even though most of the inorganic nutrients get quickly transformed into organic matter once upwelled to the euphotic layer along the coast, a substantial fraction remains unused. Together with these unused nutrients, about 36% of the organic matter produced within the nearshore 100 km gets laterally exported toward the open ocean, mostly in southwestward direction. This leakage of inorganic nutrients from the coastal zone and the continuous recycling of organic matter along the way support up to 24% of the overall observed production at a distance of 500 km from the coast. This set of processes linking the origin, biological transformation, and fate of nutrients support the growing view of the biological pump being an inherently three-dimensional process.

Plain Language Summary The upwelling of deep, nutrient-rich waters driven by winds facilitates high levels of biological production along the West Coast of continents. It is not well known, however, where exactly the nutrient-rich waters come from, and where the organic matter that is produced eventually ends up. Here we use a high-resolution numerical model to address questions about the origin, the transformation, and the fate of water masses that travel through the coastal California Current System. We find that more than 80% of the nutrients that sustain the coastal ecosystem originate from central offshore regions and from around the Southern California Bight. But biology does not completely use up the nutrient resources in the coastal environment. Together with organic matter, the unused nutrients are actually transported offshore into the open ocean. Both organic matter and nutrients arriving from coastal environments hence support the open ocean ecosystem and add to the carbon sequestration there. These processes of coastal production, offshore transport, and subsequent sequestration and subduction of carbon and nutrients, respectively, draw a fully three-dimensional picture of how carbon and nutrients are exchanged between the open ocean and coastal regions in general, and in particular in the California Current System.

1. Introduction

When averaged over large spatial and long temporal scales, the surface to deep ocean export of organic carbon and nutrients, that is, the biological pump (Ducklow et al., 2001), has to be balanced by an upward supply of inorganic carbon and nutrients to the euphotic layer. In such a simplified one-dimensional view of the ocean's biological pump, the export of organic nitrogen (and thus carbon) to depth equals the vertical supply of inorganic nitrogen to the euphotic layer and the subsequent new production within it (Figure 1a; Eppley & Peterson, 1979; Sarmiento & Gruber, 2006). This paradigm of equating new production with (vertical) export production has been extraordinarily successful in guiding research on the biological pump for the past decades and was the founding principle of much of the work undertaken during the Joint Global Ocean Flux Study Program (Scientific Committee of Oceanic Research, 1990). Most importantly, it also permitted the synthesis of a diverse set of approaches to quantify the magnitude of the biological pump, that is, export

production, and its relationship to primary production (e.g., Dunne et al., 2005; Laws et al., 2000). However, a one-dimensional view is not adequate in many ocean environments, where the lateral advection of both organic and inorganic constituents alters this balance locally, that is, results in a spatial decoupling of export production from new production (Figure 1b; Olivieri & Chavez, 2000; Plattner et al., 2005; Stukel et al., 2011; Williams & Follows, 2003). This decoupling of the upper branch of the ocean's biogeochemical loop driven by the biological pump (Sarmiento & Gruber, 2006) requires also a decoupling of the lower branch. An inorganic nutrient molecule that is freshly generated by remineralization will not be transported back to the surface where it was just formed. Instead, it likely takes a complex journey back to close the entire loop (e.g., Holzer & Primeau, 2008).

Throughout the last 30 years, the growing awareness of this spatial decoupling has led the research community from early assessments of the biological pump at global scales (Berger, 1989; Eppley & Peterson, 1979; Martin et al., 1987) to more regional investigations that unraveled more and more of the complex three-dimensional nature of the biological pump. Many individual studies have contributed to our current understanding of its spatiotemporal dynamics and the various processes that govern it. Current estimates of the strength of the biological pump range from around 5 Pg C/year (Henson et al., 2011; Siegel et al., 2014) to about 10–12 Pg C/year (Dunne et al., 2007; Laws et al., 2000; Schlitzer, 2004). It is now assumed that about 20% of this carbon sequestration flux is caused by circulation-driven exports of both dissolved and particulate organic matter (Hansell et al., 2009; Stukel et al., 2017), a process that has not received much attention in early assessments of the biological pump (Lévy et al., 2013). At regional scales, the circulation-driven exports render the biological pump highly variable in space and time. This is particularly important in regions of high eddy-kinetic energy, where most of the dynamically driven export is associated with mesoscale to submesoscale frontal subduction (e.g., Gruber et al., 2011; Krause et al., 2015; Lévy et al., 2012; McGillicuddy, 2016; Nagai et al., 2015; Omand et al., 2015; Stukel et al., 2017).

Ocean environments that are characterized by strong advective fluxes and intense mesoscale variability, such as continental margins in general, and Eastern Boundary Upwelling Systems (EBUS) in particular, are thus especially prone to experience a complex structure of the biological pump. These narrow strips of water at the interface between the land and the vast open ocean characterized by high nutrient inputs and intense biogeochemical cycling have potentially strong impacts on the global cycling of carbon and nutrients (e.g., Bauer & Druffel, 1998; Biscaye et al., 1994; Liu et al., 2010; Thomas et al., 2004; Walsh, 1991). Lateral transports of both organic and inorganic constituents to and from these systems set up local imbalances of nutrient supply, new production, and export production (Figure 1b). Such lateral transports are particularly facilitated in EBUS owing to their mean and mesoscale circulation features that lead to efficient and far-ranging cross-shore exchanges (e.g., Combes et al., 2013; Davis et al., 2014; Gruber et al., 2011; Lovecchio et al., 2017; Nagai et al., 2015; Pelegrí et al., 2005).

The offshore transport of material properties from the coastal to the open ocean has many consequences beyond making the ocean's biological pump three-dimensional. For example, the export of large amounts of organic matter from the coastal into the open ocean facilitates offshore productivity through products of remineralization processes, that is, through regenerated production (Dugdale & Goering, 1967). Enhanced concentrations of dissolved organic matter downstream of major EBUS, for example, have been shown to contribute to the regenerated productivity in oligotrophic waters along the margins of the gyres, far downstream from the actual formation of the respective organic matter (Letscher et al., 2013). Such allochthonous supplies of dissolved organic matter to the open ocean can result in export production exceeding new production in offshore regions, while in coastal areas the opposite holds true. The concurrent lateral export of particulate organic matter from the coast further exacerbates this imbalance, as it adds to enhanced open ocean export production and displaces the associated remineralization fluxes offshore (Lovecchio et al., 2017). This also affects the level of autotrophy and heterotrophy. For the Canary Current System, for example, it has been shown that the net lateral convergence of organic matter stemming from the offshore transport fuels strong heterotrophic conditions throughout the whole water column for much of the eastern subtropical North Atlantic (Lovecchio et al., 2017).

A further important consequence emerges from the potential lateral export of inorganic nutrients from EBUS (e.g., Gruber et al., 2011; Lachkar & Gruber, 2011). This leakage, possibly strengthened by mesoscale features that enhance the subduction of the nutrients before they can be consumed, has been shown to reduce coastal production by 20–40% (Gruber et al., 2011). In turn, this leakage supports enhanced offshore production.

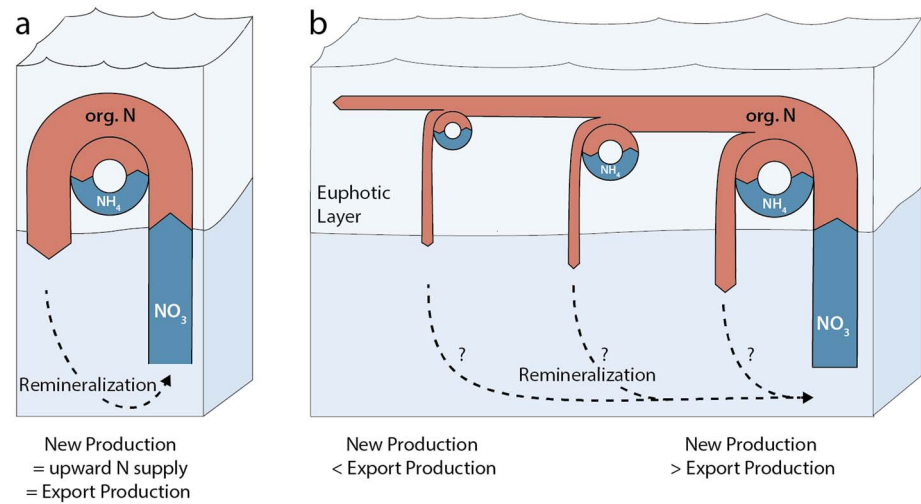


Figure 1. Schematic representations of the functioning of the biological pump. (a) One-dimensional view of nutrient supply, organic matter production within the euphotic layer, and subsequent export of organic matter fueling ocean interior remineralization. All processes act locally and averaged over a full annual cycle, new production = net community production = export production. (b) Three-dimensional view of the biological pump in regions, where lateral advective fluxes alter the local balance of nutrient supply, organic matter formation, and export production at the base of the euphotic layer (shown are two dimensions). The closing of the biogeochemical loop through remineralization processes feeding the deep reservoir of inorganic nutrients is only achieved on larger spatial scales.

This has also been reported by Pennington et al. (2010), who conclude that up to 17% of the nitrate upwelled along the central U.S. West Coast escapes the transformation to organic matter and get transported from the coastal upwelling zone into the open ocean.

Despite the recent progress in our understanding of the role of this lateral exchange, several questions remain unanswered. Where do the nutrients that support the high levels of coastal productivity come from? How do they get transformed and what is the fate of these transformation products given the strong advective character of the environment? How much carbon and nutrients are actually being exchanged?

Addressing these questions has remained a challenging task, as adequate quantification of the associated transport fluxes and characterization of water mass trajectories is needed. Unfortunately, observation-based records only allow for a very limited assessment of lateral transports due to the high spatiotemporal variability inherent in coastal environments (Ducklow & McCallister, 2004). Modeling approaches, on the other hand, need sufficient spatial resolution to represent the coastal dynamics and large model domains to assess long-range connections between coastal and open ocean regions. Only thanks to recent model developments improving upon coarse resolutions and overcoming challenges of limited model domains are we now in the position to assess the origin, transformation, and fate of nutrients supplied to a coastal environment.

Here we use a basin-scale high-resolution modeling framework applied to the California Current System (CalCS), which serves as an example to address the challenges associated with quantifying the three-dimensional nature of the biological pump. We present a model-derived nitrogen budget for the central California coast to quantify both the organic and inorganic transport fluxes that together constitute parts of the biological pump. This work expands on previous studies characterizing the spatial decoupling of export and new production within the CalCS (e.g., Nagai et al., 2015; Plattner et al., 2005) in the following points: First, we apply a much more complex ecosystem model than previous studies. This model considers, for example, also dissolved organic carbon and hence captures circulation-driven contributions to the carbon sequestration in deep waters. Second, the assessment of the lateral connectivity of the coastal ecosystem with the open ocean is made possible by our domain covering the whole Pacific basin while maintaining full eddy-resolving resolution off the U.S. West Coast. Third, we complement our Eulerian assessment of lateral transport fluxes with a Lagrangian perspective that illustrates the full extent of the three-dimensional biological pump in a manner hitherto not shown. Our results thus advance the current understanding of the dynamic and highly productive environment of the CalCS and promote a three-dimensional mechanistic

picture of nitrogen (and thus carbon) cycling within EBUS. As such, the results have important implications on current implementations of coastal environments within Earth System Models.

2. Data and Methods

2.1. Coupled Regional Oceanic Modeling System (ROMS-BEC)

We use a coupled model configuration consisting of the UCLA-ETH version of the Regional Oceanic Modeling System (ROMS; Marchesiello et al., 2003; Shchepetkin & McWilliams, 2005) as the physical component and an enhanced version of the biological elemental cycling (BEC) model (Moore et al., 2013). Solving the primitive equations of flow, the physical model component computes the evolution of the prognostic variables surface elevation, barotropic and baroclinic horizontal velocity components, potential temperature, and salinity, thereby neglecting explicit horizontal diffusion. The model runs on curvilinear horizontal coordinates and encompasses 64 terrain-following vertical coordinates in our setup. Surface and bottom refinements along the vertical axis grant appropriate representations of the corresponding boundary layer processes. Vertical mixing processes are computed using a nonlocal, K-Profile parameterization (Large et al., 1994).

Our version of the biogeochemical-ecological component, BEC, stems from the Community Climate System Model version 4 (Gent et al., 2011) and was coupled to ROMS by Frischknecht et al. (2017). BEC models the cycling of carbon, and four limiting nutrients (N, P, Fe, and Si) that govern the growth of three phytoplankton functional types (small phytoplankton, diatoms, and diazotrophs). The phytoplankton are in turn grazed by one zooplankton type. Most processes within BEC are modeled using a fixed stoichiometry assuming a small plasticity of phytoplankton with regard to their nutrient and carbon requirements. For the purpose of this study, we sum up the individual phytoplankton types to represent the total phytoplankton biomass. The model version used here is essentially the same as the one employed by Frischknecht et al. (2017) but was extended to explicitly account for the sinking of particulate matter. Numerically, this is facilitated using a piecewise parabolic method (Carpenter et al., 1990; Colella & Woodward, 1984) to compute the associated mass fluxes of particulate organic carbon and ballasting minerals (Armstrong et al., 2002). This routine has been used already in previous ROMS applications (Gruber et al., 2006) and its specifics, such as the parametrized sinking and remineralization (see also Lima et al., 2014; Moore et al., 2013; Moore & Braucher, 2008), are described in more detail in the supporting information. This model development step was necessary in order to represent better the lateral fluxes of particulate matter, which constitute an important pathway of export, particularly in EBUS (e.g., Buesseler, Antia, et al., 2007; Lovecchio et al., 2017; Nagai et al., 2015; Siegel et al., 2008). Previous versions of BEC employed an implicit, instantaneous sinking and redistribution of particulate matter throughout the water column (Moore, Doney, & Lindsay, 2004) and thus did not allow for a quantification of the lateral transports of organic and inorganic particulate forms. The burial of particulate organic matter that reaches the seafloor is parameterized following Dunne et al. (2007).

2.2. Model Setup and Simulations

Our ROMS-BEC model setup uses a telescopic grid that encompasses the whole Pacific basin but includes a strong horizontal grid refinement toward the U.S. West Coast (Figure 2a). The horizontal grid spacing ranges from 60 km around Australia to 4 km off central California. The grid thus allows for a full eddy-resolving representation of the very dynamic coastal environment, while still capturing basin-wide oceanic and atmospheric teleconnections (see Frischknecht et al., 2015, 2017). In addition, this model setup reduces the challenges of providing adequate lateral open boundary conditions by moving them far away from the region of interest. Finally, this basin-scale setup permits us to study the long-range transport of material properties to and from the U.S. West Coast in a way that a traditional regional grid would not allow for.

With respect to Frischknecht et al. (2017), the parameter set governing the biogeochemistry has been adjusted to reach better agreement with observation-based estimates of production and export. In particular, we have reduced the maximum growth rates and the particulate organic carbon remineralization rate (which effectively increases the associated dissolution length scale) to alleviate production biases compared to previous applications. The parameter set is documented in Table S1 in the supporting information. Our setup now also includes climatological riverine inputs of freshwater (Dai et al., 2009) and nutrients (Beusen, 2014), as well as atmospheric deposition of nitrogen (Lamarque et al., 2013). Additionally, the model includes a new parameterization for benthic iron fluxes (Dale et al., 2015) that depends on the sedimentary carbon oxidation rates and bottom water oxygen concentrations and is based on a comprehensive observational data set (most of which stem from measurements along the U.S. West Coast).

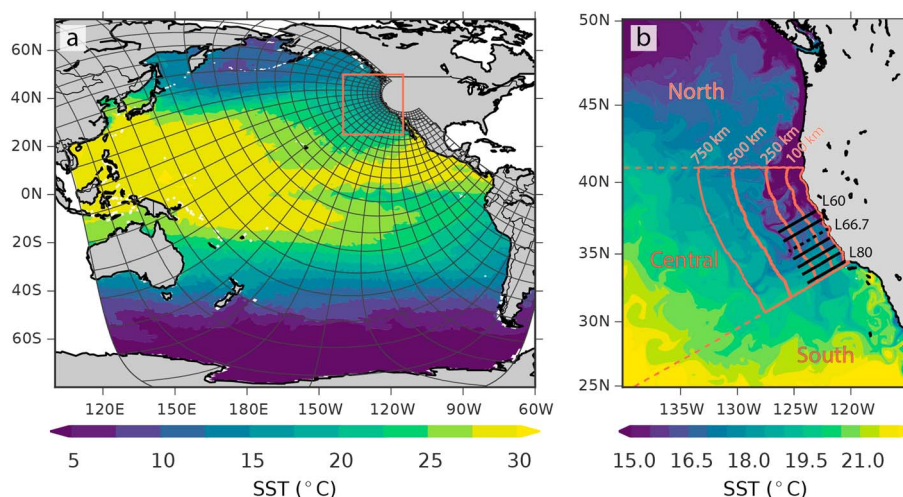


Figure 2. Numerical grid and analysis domains with a snapshot of sea surface temperature (SST) in the background. (a) Numerical grid encompassing the whole Pacific basin with substantial horizontal grid refinement toward the region of interest, that is, the California Current System (highlighted red square). (b) Close-up with budget analysis domains for the central California Current System and dashed lines indicating latitude separated regions used in the analyses. Black lines represent measurement arrays used for model evaluation. Background SST field stems from 1 August of the first year after the completed spin-up.

Initial and boundary conditions were derived from different observation- and model-based data products. Temperature, salinity, and nutrient distributions are based on World Ocean Atlas 2013 (Levitus et al., 2014). Those for dissolved organic nutrients, ammonium, and iron were initialized from climatological runs of a global CESM simulation (Yang et al., 2017). Phytoplankton and zooplankton biomass were estimated from climatological surface chlorophyll distributions derived from SeaWiFS (<https://oceandata.sci.gsfc.nasa.gov/SeaWiFS/>, last accessed 8 February 2018) and extrapolated to depth following the procedures detailed in Morel and Berthon (1989). The open boundary conditions for currents and sea surface height (SSH) are based on SODA 1.4.2 (Carton & Giese, 2008) north of 24°S and a climatological ROMS simulation covering the whole Southern Ocean south of this latitude (Haumann, 2016).

We first spun up the physical core from rest for 10 years using as surface forcing the climatological mean fields of wind stress, solar short-wave radiation, and fluxes of heat and freshwater derived from ERA-Interim (Dee et al., 2011). In order to expose the model to higher-frequency variability, we modified these climatological fields by adding daily anomalies of the year 2001, that is, created a normal year forcing data set (Large & Yeager, 2009; see also the supporting information). ERA-Interim short-wave and heat fluxes have been shown to contain biases, in particular, in EBUS, where low-level cloud cover reduces incoming short-wave and outgoing long-wave radiation (Brodeau et al., 2010). We address this issue by correcting these fields following the methods developed by the Drakkar community (Dussin et al., 2016).

After 10 years of physical spin-up, we turned on BEC and extended the spin-up for another 10 years. Subsequent to the complete 20-year spin-up, we ran a 10-year simulation for analysis purposes with two different output frequencies in order to characterize the mean state (monthly mean output) and the inherent high-frequency variability (daily mean output). Although relatively short, this spin-up is sufficient for the upper 500 m of the water column to reach cyclostationarity with only a minimal amount of drift (see supporting information). We avoided a longer spin-up in order to ensure that the model stays relatively close to the observation-based initial conditions.

2.3. Eulerian Versus Lagrangian Framework

We employ two complementary analysis approaches: First, we assess the mean production and redistribution of organic and inorganic constituents within the CalCS using an Eulerian framework. This analysis builds up toward a model-derived nitrogen budget for the central CalCS. Second, we complement these findings using a Lagrangian analysis framework focusing on the water masses that support high coastal productivity. We uncover their pathways toward the coastal upwelling system and their onward journey into the open ocean and investigate the biogeochemical transformations that occur along these trajectories.

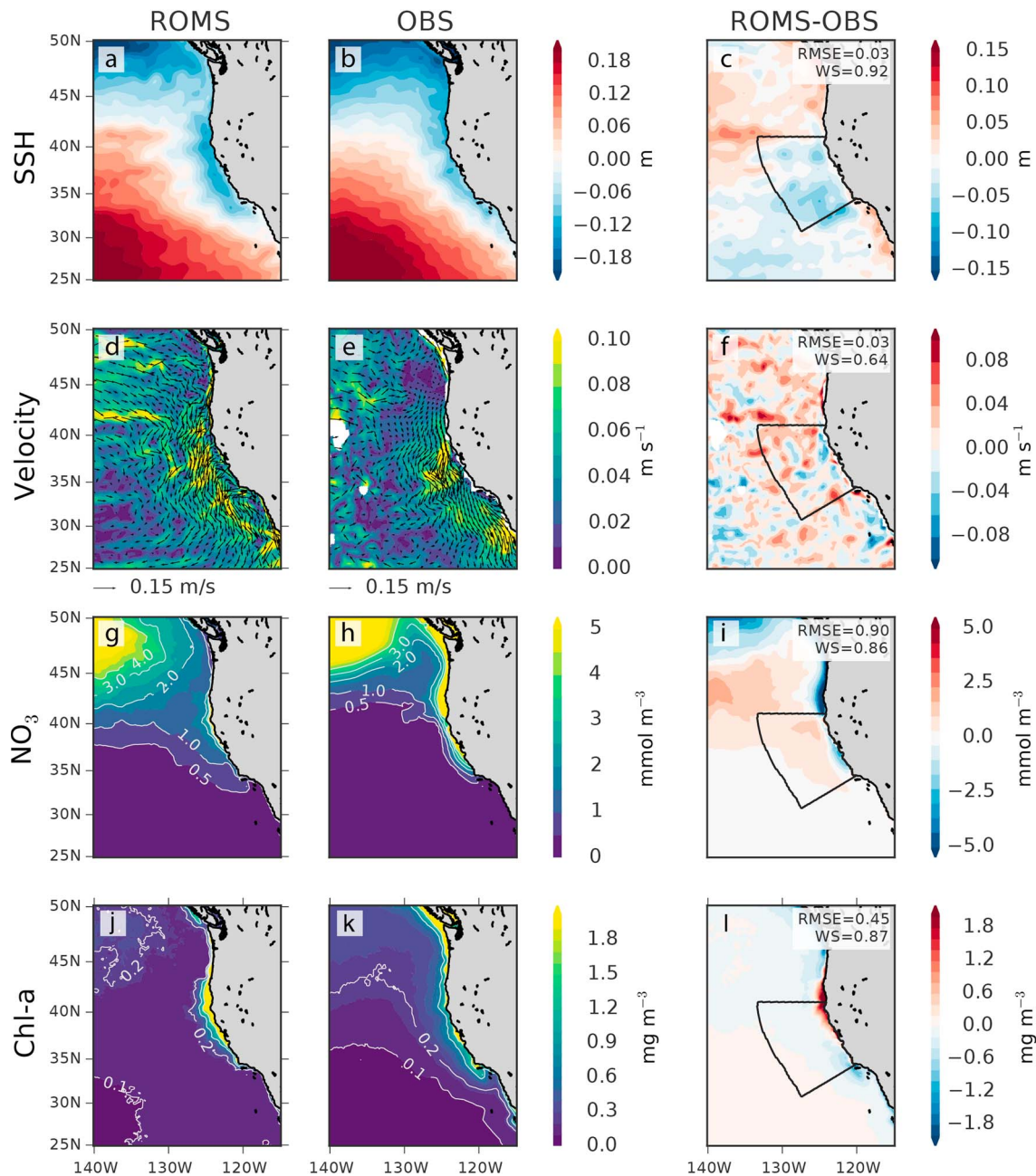


Figure 3. Modeled and observed surface ocean properties in the Northeast Pacific. The individual plots depict time-mean distributions derived from (left) model and (middle) observations, and (right) their difference for (a–c) sea surface height (SSH), (d–f) surface velocity and corresponding currents, (g–i) NO_3 , and (j–l) chlorophyll a (Chl-a). Observational data are provided by CMECS for SSH (<http://marine.copernicus.eu/>), the Global Drifter Program for velocity and currents (<http://www.aoml.noaa.gov/phod/dac/dacdata.php>), CSIRO for NO_3 (<http://www.data.gov.au/no/dataset/cars-2009-csiro-atlas-of-regional-seas>), and globcolour for Chl-a (<http://www.globcolour.info/>). The text box in the top right corner of each difference panel indicates the root-mean-square error (RMSE) and the Willmott skill score (WS, where 1 (0) indicates complete (dis)agreement; Willmott, 1981) for the California Current System budget analysis region (black outline).

The latter analysis approach is based on the offline particle tracking tool ARIANE (Blanke & Raynaud, 1997 available through <http://stockage.univ-brest.fr/~grima/Ariane/>). We generated an extensive trajectory database consisting of ~ 1.4 mio trajectories. Particles were seeded on 90 randomly selected days through the years 2–9 of the analysis run in grid cells located within 100 km distance of central California. To tag only water masses that sustained high production, the seeding was undertaken only if the phytoplankton concentration exceeded 10 mmol C/m^3 in the daily mean. This threshold represents about the 90th percentile within the coastal zone and corresponds to roughly $3 \text{ mg chlorophyll/m}^3$. Subsequent to the seeding, we computed

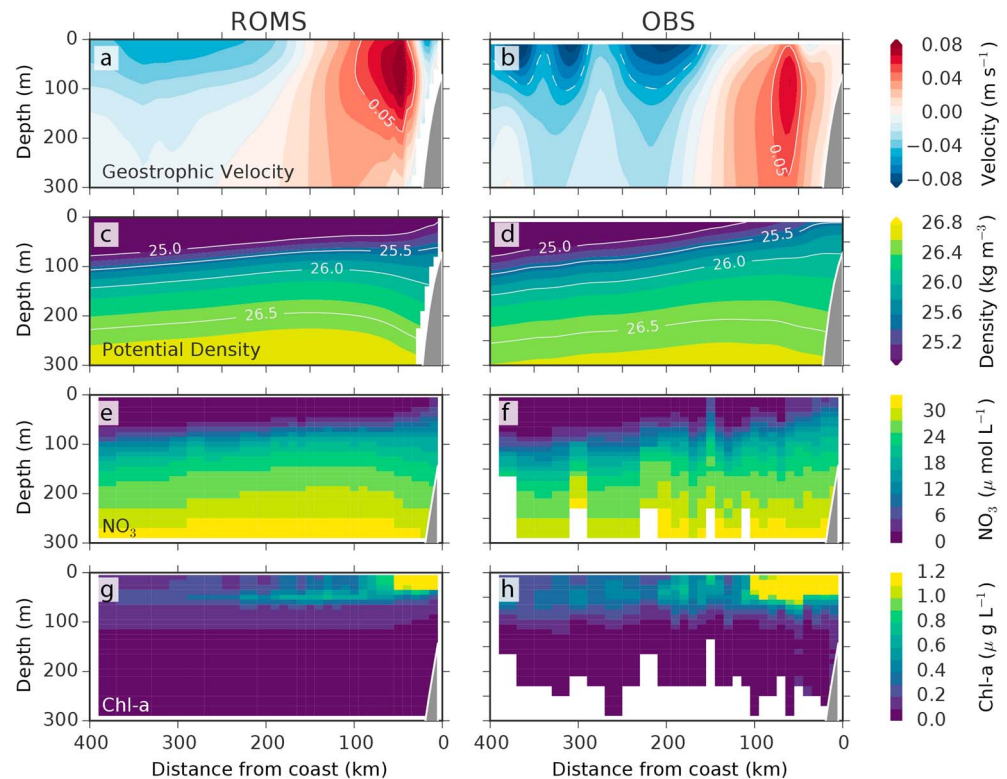


Figure 4. Vertical offshore sections of annual mean properties off the coast of Central California. Shown are modeled and observed (a, b) alongshore geostrophic velocity, (c, d) potential density, (e, f) NO_3 , and (g, h) Chl-a along lines of the California Cooperative Oceanic Fisheries Investigation (CalCOFI) observational network in central California (33–38°N; see Figure 2b). Observational data for geostrophic velocity and potential density are taken from the California Underwater Glider Network (Rudnick et al., 2017) along Line 66.7 of the CalCOFI network. In situ measurements for NO_3 and Chl-a are compiled from Line 60 to Line 80 climatologies of the CalCOFI network (<http://calcofi.org/data.html>).

both backward and forward trajectories for all particles on daily mean model output fields every 3 days for ± 360 days. This produces a 720 days record of the evolution of physical and biogeochemical properties for each of the seeded particles.

The choice of this threshold value has little impact on our conclusions regarding the pathways water masses take toward and from the central California coast, but it does affect the biogeochemical transformation rates captured by the Lagrangian analysis. Different thresholds yield differences in the magnitude of the peak in production and biomass. A reduction of the threshold, for example, would dilute the peak in production (see Figure 11b) as a result of the seeding of an increasing amount of particles in waters experiencing lower productivity. The respective production would be predominantly facilitated through the recycling of organic matter, that is, regenerated production, and would therefore not represent those water masses supplying new nutrients to the euphotic layer. Given our interest in upwelling particles causing high rates of new production associated with upwelling, we thus decided in favor of a relatively high threshold.

3. Model Evaluation

The evaluation of the model's performance against observation-based estimates for the physical and biogeochemical environment in the Northeast Pacific demonstrates the model's ability to reproduce the features that characterize the CalCS region (Figure 3). The model adequately simulates zonal and meridional gradients in SSH, reflecting the overlying atmospheric forcing that drives the California Current and grants upwelling favorable conditions along the U.S. West Coast. The offshore intensification of the southward current, in particular, off central California, suggested by surface drifter data, is well captured in the model solutions. The resulting upper ocean divergence along the coastline is balanced by the upwelling of deep, cold, and nutrient-rich water masses, reflected also in negative SSH anomalies, cold SSTs hugging the central California coastline (Figure 2b), elevated levels of nutrient concentrations (e.g., nitrate), and biomass proxies (e.g., chlorophyll a).

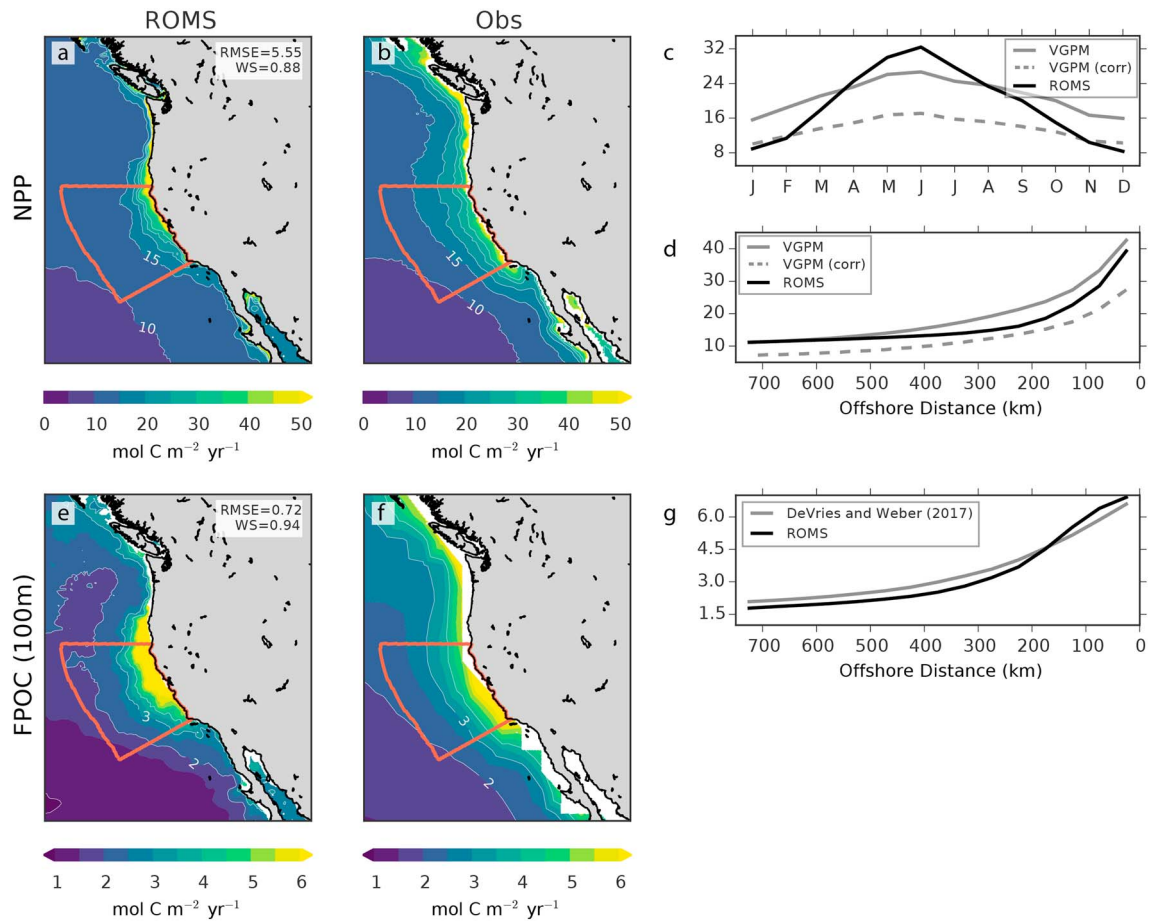


Figure 5. Production and export estimates along the North American continent. (a) Modeled and (b) observation-based estimates of annual mean Net Primary Production (NPP). The panels to the right illustrate (c) the seasonality and (d) the annual mean cross-shore gradient in NPP for the region highlighted in red. Observation-based estimates are derived from the Vertically Generalized Production Model (VGPM; Behrenfeld & Falkowski, 1997) applied to data obtained from the SeaWiFS. Black lines refer to ROMS, gray lines are derived from SeaWiFS-VGPM (dashed lines applying a California Current System-specific correction following Kahru et al., 2009). The bottom plots show particulate organic carbon (POC) flux estimates at 100 m derived from (e) ROMS and (f) the data-assimilative model by DeVries and Weber (2017). Panel (g) compares the cross-shore gradient of POC fluxes for the two products. All fluxes are reported in $\text{mol C m}^{-2} \cdot \text{year}^{-1}$.

The surface characteristics of the CalCS extend into the water column revealing the complex interplay of physical and biogeochemical processes (Figure 4). Comparing our model results to observational records from the California Cooperative Oceanic Fisheries Investigations (CalCOFI, <http://calcofi.org/>) or the more recently installed California Underwater Glider Network (Rudnick et al., 2017) reveals good agreement in general with regard to the cross-shore gradients of physical and biogeochemical properties off central California.

Our model captures the location and surface refinement of the equatorward flowing California Current. The model solutions also agree on the position and extent (both lateral and vertical) of the California Undercurrent located at the shelf break. While the model slightly underestimates the geostrophic velocity component in the offshore California Current, the flow associated with the California Undercurrent seems to be too strong and surface intensified compared to observational records (Figures 4a and 4b). This is likely a response to the atmospheric forcing product that is relatively coarse in horizontal resolution and hence underestimates the coastal wind dropoff that proves crucial to set coastal circulation dynamics (e.g., Capet et al., 2004; Renault, Hall, & McWilliams, 2016). The model response to this wind forcing results in an offshore minimum of SSH (Figure 3), which favors a stronger geostrophic poleward flow. Reflecting this balance of equatorward and poleward flow, the isopycnals exhibit stronger than observed tilting in the upper water column in the very nearshore region, coinciding with the poleward flow anomaly. Besides this shortcoming, the isopycnal tilting (with upper ocean upward and deep downward tilt) is generally well reproduced. This is a feature that is characteristic to coastal upwelling environments and co-occurs with the supply of high nutrient contents to the surface coastal ocean (Figures 4c–4f).

The nutrient input fuels productivity in the surface layers, which builds up particularly high biomass close to the coast with a slightly deeper maximum in offshore regions (Figures 4g and 4h). These characteristics are largely well reproduced, though the model tends to underestimate surface nitrate in nearshore regions, while the opposite is the case in offshore environments. The low bias in coastal nitrate coincides with slightly overestimated surface chlorophyll levels (Figure 3) and a more pronounced summer peak in productivity with respect to satellite-based estimates (Figure 5c). Besides that, the spatial pattern and seasonal cycle of net primary production (NPP) in the CalCS are generally captured well. The associated carbon export in the CalCS estimated from the model, and in particular, its pronounced cross-shore gradient seems to be well supported by both data-assimilative model estimates (DeVries & Weber, 2017; Figures 5e–5g) and in situ measurements from the Southern California Bight (Berelson & Stott, 2003; Munro et al., 2013; see supporting information). Also, the burial efficiency of the organic matter lies within the range of observational estimates (e.g., Berelson & Stott, 2003; Jahnke, 1990). For example, in the nearshore, shallow areas along central California (<100 km and <100 m), about 50% of the particulate organic matter that reaches the seafloor is lost to the sediment.

Additional model evaluation using various observation-based data sets is provided in the supporting information. It includes Taylor diagrams (Taylor, 2001) for surface ocean and vertically integrated properties (Reynolds et al., 2007; Ridgway et al., 2002), nutrient and oxygen profiles (Garcia et al., 2013a, 2013b), primary production estimates (Smith & Eppley, 1982), and particulate organic carbon flux estimates (Buesseler, Lamborg, et al., 2007; Devol & Hartnett, 2001; Honjo et al., 1995; Knauer et al., 1984; Martin et al., 1987; Wong et al., 1999) compiled by Laufkötter et al. (2017).

Despite the considerable increase in the degrees of freedom given the moving away of the lateral boundary conditions and the strong increase in ecosystem complexity, this model still performs on par with our previous work that employed a regional U.S. West Coast configuration of ROMS and a simpler NPZD-type ecosystem/biogeochemical model (Gruber et al., 2006, 2011; Nagai et al., 2015). In general, while recognizing some fallacies, the model performs well and reproduces the important characteristics of coastal upwelling as well as the complex structure across the gradients in offshore direction. Hence, we consider the model well suited to investigate the cross-shore exchanges of carbon and nutrients within the CalCS.

4. The Eulerian Point of View: From Production to Export

A central tenet of the one-dimensional view of the ocean's biological pump is the equality of new production (NP), that is, the organic matter formation supported by new nitrogen, primarily in the form of NO_3 (Dugdale & Goering, 1967); net community production (NCP), that is, the balance between primary production and heterotrophic respiration and remineralization; and (vertical) export production (EP), that is, the organic matter exported vertically by sinking and advection across 100-m depth (Figure 1a). In the model, these fluxes are diagnosed from the corresponding biogeochemical processes at every time step and then averaged to monthly mean values.

Our starting point for the investigation of the three-dimensional nature of the biological pump is the analysis of the annual mean of these three fluxes, as differences between them are a clear indication of the importance of lateral transport that decouples EP from NCP and NP. We integrate NP and NCP over the top 100 m and compare the resulting fluxes with the net export flux of organic matter across the 100-m isosurface (EP). This depth roughly corresponds to the average euphotic zone depth in our analysis domain. We use nitrogen as a basis for our analyses, but note that owing to the fixed stoichiometric C:N ratio in our model (116 to 16), the organic nitrogen fluxes correspond directly to organic carbon fluxes.

4.1. Local Imbalances of Production and Export Along the U.S. West Coast

In the annual mean, the coastal and curl-driven upwelling supplies large amounts of total inorganic nitrogen (TIN), mostly in the form of NO_3 , to the nearshore areas of the U.S. West Coast, fueling high levels of NP there (Figures 6d–6f). But the intensity of NP tapers off quickly with increasing distance from the coast, even though levels remain well above 0 in offshore waters way beyond the coastal upwelling zone. The distribution is very different for both NCP and EP. High levels of NCP are confined to a narrow coastal strip of water, whereas further offshore, NCP is essentially zero. Thus, with the exception of a narrow strip along the coast, NP exceeds NCP throughout the investigated domain. The spatial pattern of EP reflects these cross-shore gradients in NP and NCP and also reveals imbalances with respect to these two fluxes. As is the case for NP and NCP, the coastal regions also have the highest EP, but its magnitude is substantially smaller. This implies that only a fraction

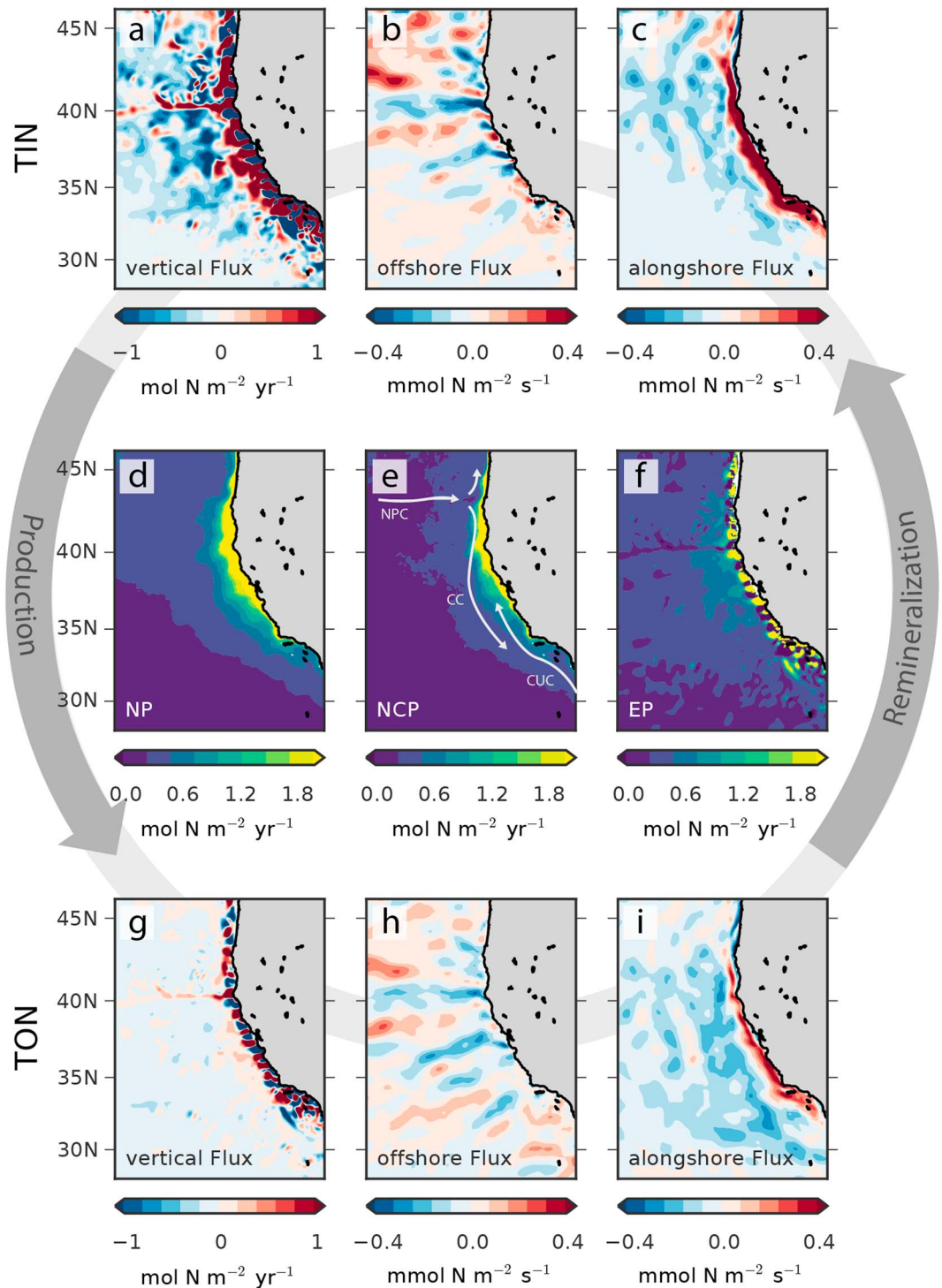


Figure 6. Transport, production, and export of nitrogen in the California Current System. (a–c) Vertical and lateral advection fluxes of total inorganic nitrogen (TIN). (d–f) New production (NP), net community production (NCP), and export production (EP). (g–i) Vertical and lateral advection fluxes of total organic nitrogen (TON). Vertical fluxes are reported at 100-m depth, lateral fluxes represent top 100-m averages, and production terms are integrated over the top 100 m. Arrows in the NCP panel indicate the relevant circulation features, that is, the North Pacific Current, the California Current, and the California Undercurrent. Gray circular arrows indicate the close link between transport, transformation, and export processes.

of the organic matter that is produced within the top 100 m is locally exported to depth. In regions further offshore, EP actually exceeds both NCP and NP.

This strong decoupling between NP, NCP, and EP implies a substantial lateral transport of organic matter. The model-diagnosed offshore fluxes of total organic nitrogen (TON) in the top 100 m, that is, the sum of all forms of particulate and dissolved organic nitrogen, are indeed quite intense (Figure 6h), but there are also distinct regions with onshore fluxes in the annual mean. In fact, the cross-shore fluxes are organized in zonal bands of offshore and onshore transports describing efficient exchange pathways between the nutrient replenished coastal areas with high biomass and the offshore oligotrophic open ocean (see also Nagai et al., 2015). Along the central U.S. West Coast, the net effect of these zonally organized exchanges is a far-reaching offshore transport of organic matter from coastal to open ocean environments. Superimposed on the zonally organized cross-shore exchanges are alongshore fluxes of TON (Figure 6i). They are mainly associated with two major circulation features within the CalCS. The coastally confined poleward flowing California undercurrent advects TON along the California coastline. In contrast, the broader but less intense flow associated with the California Current located further offshore advects organic matter along the eastern boundary of the ocean basin toward the equator. Finally, vertical advective fluxes of TON can alter the local balance of NP, NCP, and EP as well (Figure 6g). Along the coastline, vertical advective fluxes of TON across 100 m depth are most intense and describe alternating upward and downward drafts associated with upwelling cells. Their net effect along the coastline is an upward directed flux of TON, augmenting the pool of organic matter available for lateral export without enhancing NCP. This pool partly stems from labile organic matter that has been exported but is upwelled again across the 100 m depth horizon before it had a chance to remineralize (see also Plattner et al., 2005). Another contribution arises from refractory dissolved organic matter (with a life time of 2.5 years), which we include in all results reporting TON. In regions further offshore, vertical advective fluxes of organic matter are directed downward and thus add to the export of TON by sinking, that is, enhance open ocean EP.

The transport fluxes of TIN strongly resemble those of TON in terms of the spatial distributions (Figures 6a–6c). However, in terms of magnitudes, the coastally confined northward flow advects waters with much higher TIN contents than TON. Moreover, the vertical fluxes of TIN are much larger than those of its organic counterpart. These differences in transport are primarily the result of the differences in the mean distribution and concentrations of inorganic nitrogen and organic matter in the CalCS and throughout the water column (Figure 7). The organic matter formation within the euphotic layer constantly depletes the pool of inorganic nutrients in surface waters. TON concentrations are thus highest within the top 50 m of the water column, and their maximum is slightly displaced toward open ocean regions and southward along with the main flow of the California Current. Those of NO_3 (the predominant component of TIN) increase very strongly with depth and are highest along the coastline. The organic matter gradient at 100 m is thus less pronounced, and hence, its fluxes across this depth are much weaker than those of TIN. Lateral fluxes of TIN furthermore outweigh those of TON, because NO_3 concentrations in the lower euphotic layer are much higher than those of organic matter.

Taken together, the Eulerian perspective reveals a system characterized by strong lateral transports of both organic and inorganic nitrogen that lead to a high degree of spatial decoupling of NP, NCP, and EP.

4.2. A Model-Based Nitrogen Budget for the Central CalCS

In our nitrogen budget for the central CalCS, the qualitatively illustrated imbalances of NP, NCP, and EP translate into quantitatively observed differences between the respective fluxes (Figure 8). Organic matter production rates are highest close to the shore and taper off with increasing distance from the coast. Between 500 and 750 km offshore, NPP per unit area is only 34% of the one observed within 100 km from the coast (see also Figure 5g). Within the first 100 km, NP contributes about 50% to this NPP, directly reflecting the strong upwelling supply of NO_3 along the coastline (Figure 6a). Moving further offshore, the NP contribution decreases rapidly with increasing offshore distance to values of less than 20% at 500 km and beyond. As the relative contribution of NP decreases, that of regenerated production, that is, the production fueled by the uptake of NH_4 stemming from the remineralization of organic nutrients, increases. At any distance beyond 100 km, regenerated production outweighs NP.

In the nearshore 100 km, NP and NCP exceed the export to depth (NCP, $\text{NP} > \text{EP}$) by a factor of 2 or more. Moving offshore, this imbalance changes in favor of EP, such that for all budget analysis boxes beyond 100 km, EP exceeds NCP. Between 100 and 250 km from the coast, this exceedance amounts to 124%, and further increases to 161% between 500 and 750 km offshore. Two mechanisms potentially support this enhanced open ocean export production. First, organic matter that is transported offshore directly adds to EP through

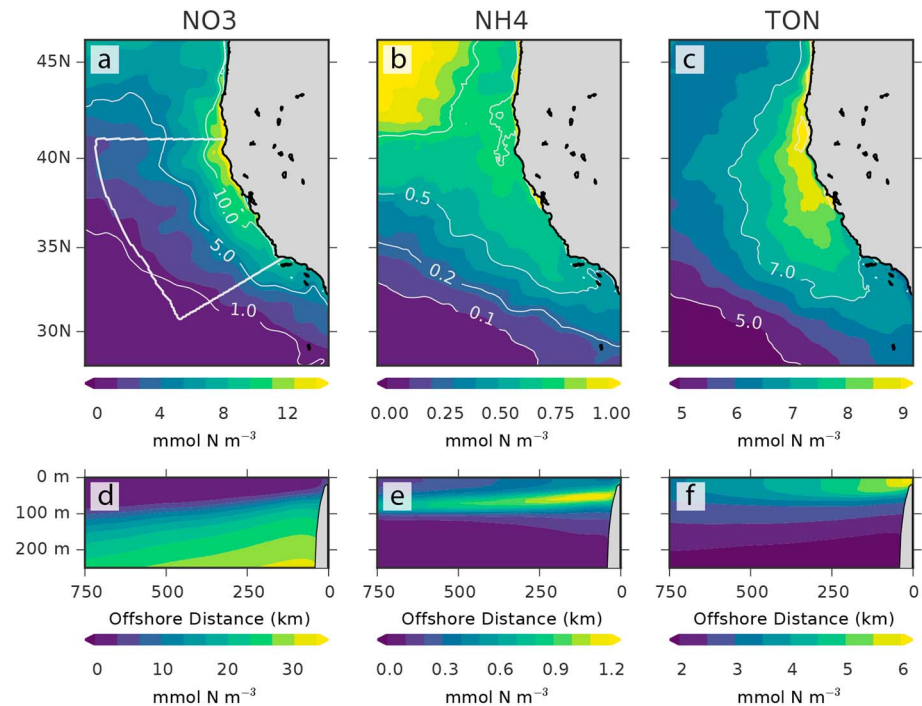


Figure 7. Nutrient and organic matter distributions in the California Current System. (a–c) Top 100-m mean distributions of NO₃, NH₄, and total organic nitrogen (TON) and (d–f) their cross-shore sections. The cross-shore section is computed from the region highlighted in (a).

the subsequent sinking in regions downstream of its origin. Second, the offshore transport of inorganic nutrient elements supports productivity in more oligotrophic open ocean environments and the sinking of the respective organic matter adds to the open ocean EP as well.

Indeed, the offshore flux of TON equals or exceeds the local NCP at every budget analysis interface in the nearshore 500 km (96% at 100 km, 215% at 250 km, and 130% at 500 km; Figure 8a). The excess lateral export of organic matter with respect to NCP is mainly sustained by lateral fluxes from the coast. The offshore transport of organic matter is dominated by the contribution of dissolved forms, which increases from 66% at 100 km to 93% at 750 km. Particulate contributions are mostly confined to nearshore regions. At 100 km from the coast, the lateral export of phytoplankton and zooplankton biomass amounts to 24% and that of particulate organic nitrogen to about 10% of the total flux. Alongshore fluxes of TON are generally weaker and less important for the organic nitrogen budget. But in the nearshore 250 km, alongshore fluxes are convergent and hence potentially support the offshore transport and the subsequent excess open ocean export. Further offshore, and associated with the California Current, alongshore fluxes are divergent and tend to transport organic matter southward. Note here that the budget does not include burial fluxes. The total loss of organic matter to the sediment, however, only amounts to 2.6% of the NCP (and hence the lateral offshore transport) within the budget analysis box closest to shore. Consequently, we consider it negligible for the key results presented here, and the conclusions drawn from them.

For inorganic nitrogen, many of these fluxes within the top 100 m have a similar pattern to those of TON (Figure 8c). Our results suggest a substantial leakage of TIN from the coastal upwelling zone into the offshore domain. Most of the lateral TIN fluxes within the top 100 m are associated with NO₃. Those associated with NH₄ only account for 6–13% and increase from the coastal region to the open ocean. This is not surprising, given their mean distributions and concentrations (Figure 7). Important differences from the organic budget arise when looking at the vertical advection. For TIN, coastal and curl-driven upwelling drive strong vertical supply fluxes into the euphotic layer within 250 km from the coast. Further offshore, this tendency reverses and inorganic nitrogen tends to be subducted below the euphotic layer at magnitudes that even exceed EP (see also Figure 6a). On the one hand, this results in a decrease of offshore TIN transport beyond 500 km within the upper 100 m that is aggravated by the continuous drawdown of nutrients through production within the euphotic zone (Figure 8b). On the other hand, the subduction of TIN fuels a deep and strong offshore

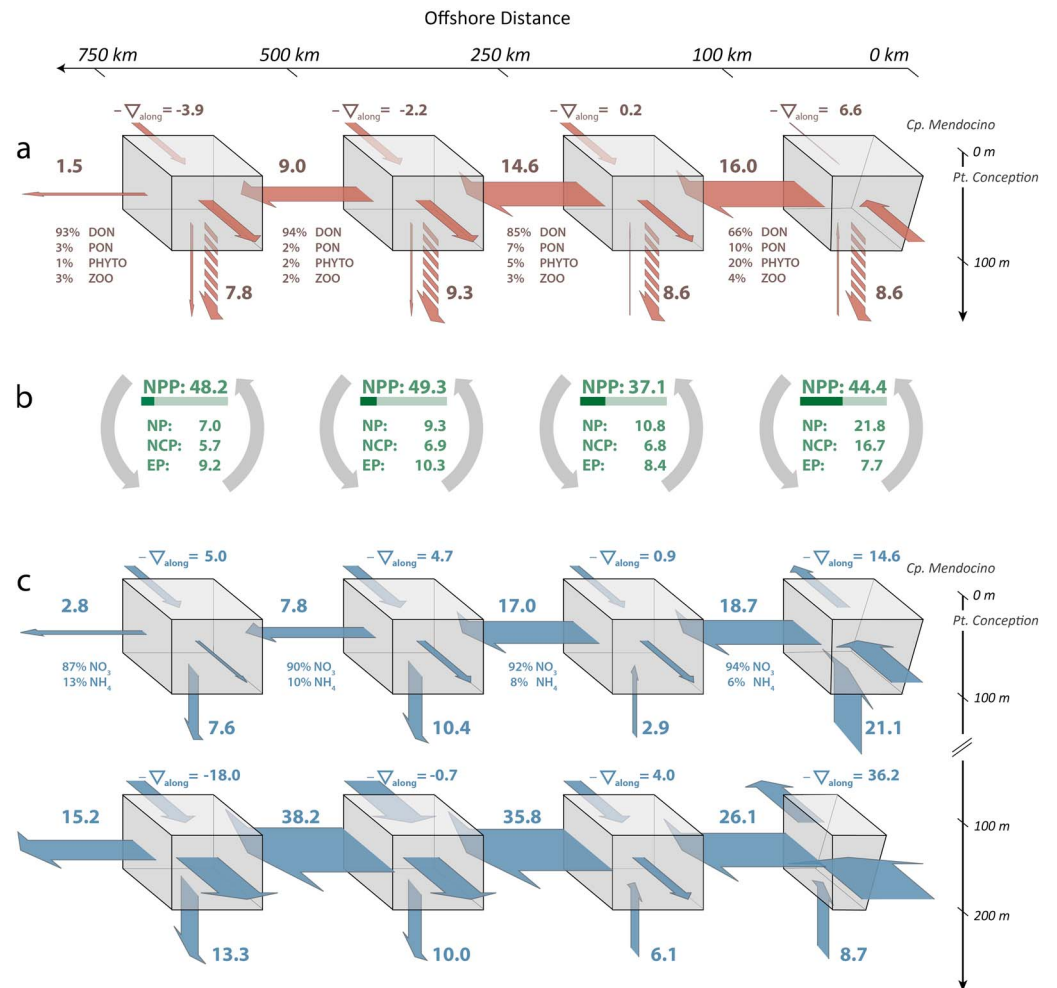


Figure 8. Model-derived annual mean nitrogen budget for the central California region (as defined in Figure 2b). (a) Total organic nitrogen transport fluxes within the top 100 m. Dashed arrows indicate sinking fluxes of particulate organic nitrogen. Contributions of the different forms of organic matter to the offshore transport are indicated in percent. (b) Organic matter formation within the top 100 m and export across 100 m integrated over the course of the year. Listed are net primary production (NPP), new production (NP), net community production (NCP), and export production (EP). The partitioning of new and regenerated production is illustrated by the colored bar (dark part corresponding to the contribution of NP to NPP). The gray arrows illustrate the close interaction of organic and inorganic nutrient cycles. (c) Advective transports of inorganic nitrogen (NO₃ and NH₄) within the top 200 m. All numbers are given in 1e10 mol N. For the alongshore direction, only the divergence of the flux is indicated above the respective box. All arrow widths are scaled to the actual magnitude of the corresponding flux. Shown are only biological transformation and physical advection fluxes (not shown are time rate of change, mixing, and diffusive fluxes).

transport of inorganic nitrogen. Similar to those of TON, alongshore fluxes of TIN are of lesser importance to the budget, with the exception of the coastal alongshore fluxes. These fluxes are substantial and their convergence in alongshore direction provides strong sources of TIN for the adjacent budget analysis boxes in offshore direction.

4.3. Discussion of the Eulerian Perspective

Our results illustrate several features highlighted by previous studies. In particular, they underpin the decoupling of EP from NP that is set up by the lateral transport within the CalCS (cf. Olivieri & Chavez, 2000; Plattner et al., 2005; Stukel et al., 2011). The starting condition is the very high levels of NCP in nearshore regions that result in a sizeable organic matter pool. A substantial fraction of this pool is readily picked up by the highly advective environment of the EBUS, leading to a strong offshore transport of organic matter that fuels EP in the offshore regions, while keeping NCP there low (e.g., Hales et al., 2006; Nagai et al., 2015; Plattner et al., 2005).

Transport processes that alter the functioning of the biological pump at regional scales are important not only in the CalCS but also in other EBUS. For the Canary Upwelling System, Lovecchio et al. (2017) reported that more than 30% of the local NCP within the coastal zone is exported offshore. An earlier estimate for the central CalCS suggested that 20% of the NP within the upwelling zone of the CalCS gets exported offshore (Pennington et al., 2010). These previous estimates are significantly lower than ours, that is, about 73% of the local NP is laterally exported, but important differences in the underlying methods exist. For example, both earlier estimates do not consider DON. Without this contribution, our estimate of lateral export from the upwelling zone reduces to only 25%, and hence is consistent with the estimate by Pennington et al. (2010). While DON thus constitutes a substantial fraction of the total offshore transport in our model simulation, the lack of corresponding observational constraints renders it a source of uncertainty. Nevertheless, including dissolved organic forms in our calculations expands on the findings of previous studies and hints at their potential importance to support offshore ecosystems and enhanced export production (cf. Letscher et al., 2013).

The elevated NP relative to NCP requires that, in addition to organic matter, also inorganic nutrients need to be transported laterally, thereby fueling NP while suppressing NCP. Indeed, the results indicate that the export of TON is accompanied by a substantial offshore transport of inorganic nitrogen from the coastal zone. This is not entirely unexpected along eastern boundaries of ocean basins, in particular, along slope dominated margins, such as the U.S. West Coast. Due to relatively short residence times on the shelf, the incomplete assimilation of nutrients supplied to the euphotic zone leaves inorganic constituents available for lateral export to the open ocean (Lachkar & Gruber, 2011). In their observation-based nitrogen budget derived from empirical relationships between nitrate and temperature, Pennington et al. (2010) estimated that approximately 17% of the upwelled nitrate along central California and within the top 60 m is transported laterally from the upwelling zone to the offshore region. For the same region, our results suggest a somewhat stronger lateral transport fraction of 31%. This is, however, not surprising given our more realistic and dynamic modeling approach.

The zonally organized cross-shore exchange pathways are characteristic to EBUS (Davis et al., 2014; Lovecchio et al., 2017; Nagai et al., 2015). They are caused by the geometry of the coastline that tends to organize the mesoscale turbulence spatially (e.g., Davis et al., 2014). Especially relevant are capes as they stimulate the generation of filaments (e.g., Barth et al., 2005, 2000; Brink & Cowles, 1991; García-Muñoz et al., 2005; Pelegrí et al., 2005), which later give rise to eddies that propagate offshore along preferred conduits. The eddies that propagate along these conduits, that is, eddy corridors, tend to dominate the far-reaching transport beyond a few hundred kilometers. In contrast, the transport for the first few hundred kilometers tends to be dominated by filaments superimposed on the mean Ekman transport (e.g., Combes et al., 2013; Lovecchio et al., 2018; Nagai et al., 2015).

Mesoscale features also enhance the subduction of inorganic and organic nitrogen (e.g., Barth et al., 2002; Gruber et al., 2011; Omand et al., 2015; Stukel et al., 2017). This mesoscale-induced subduction may also explain the demonstrated imbalance between EP and NP in EBUS, and the increasing relative contribution of circulation-driven exports in offshore regions (Figures 6a and 6g). Observations suggested that the subduction of both dissolved (Hansell et al., 2009; Lévy et al., 2013) and particulate (Omand et al., 2015; Stukel et al., 2017) forms of organic matter may contribute to ~20% to the total export. These estimates are somewhat higher than those derived from our model simulation, which suggest vertical advection-driven exports of TON of 10% and 16% of the total export at 250–500 and 500–750 km from the coast, respectively (Figure 8a).

Despite our Eulerian perspective having permitted us to establish a good quantitative understanding of the transport dynamics within EBUS that set the local imbalances of the biological pump, some questions about its functioning remain unanswered. What is the actual origin of the waters that support the high coastal production? And what is the fate of the produced organic matter that ultimately fuels EP? Answering these questions will not only expand our knowledge on the large-scale connectivity of EBUS but also reveal the full extent of the spatial connectivity of continental margins and open ocean environments. To uncover the elusive pathways of water masses that comprise the full structure of the three-dimensional biological pump along the U.S. West Coast, we thus make use of the extensive trajectory database consisting of 1.4 mio particles that we tracked forward and backward in time.

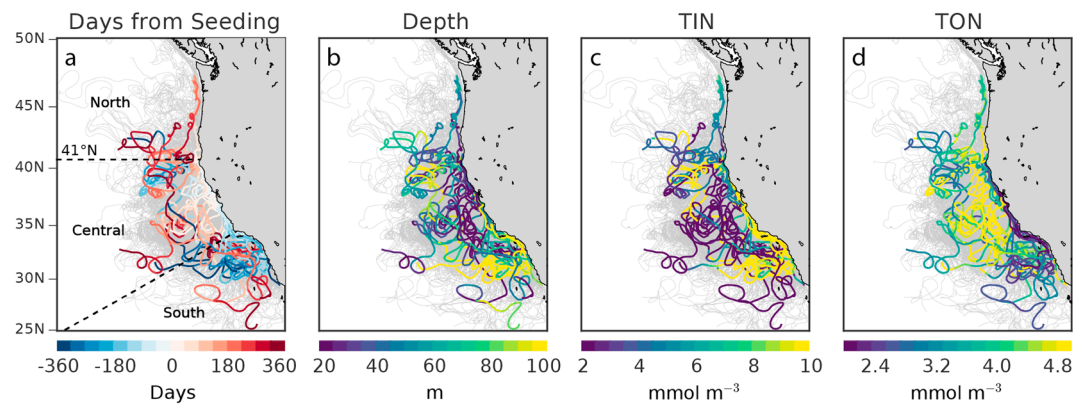


Figure 9. Illustration of the high spatiotemporal variability of particle trajectories within the CalCS. The plots show 250 randomly selected trajectories from the 1.4 mio generated through our Lagrangian experiments. Only 10 trajectories are color coded to illustrate (a) age relative to seeding, (b) depth, (c) total inorganic nitrogen (TIN), and (d) total organic nitrogen (TON).

5. The Lagrangian Point of View: Uncovering the Three-Dimensional Biological Pump in the CalCS

A first glance at a few randomly selected trajectories from the Lagrangian particle tracking experiment reveals the high spatiotemporal variability inherent in the CalCS (Figure 9). Waters contributing to the highly productive ecosystem off central California originate from a wide range of geographical locations, spanning latitudes from 25°N off Baja California to 50°N off Vancouver Island and offshore distances up to 1,000 km. Throughout their 720-day journey to and from the coastal upwelling zone, the individual water parcels, that is, the waters surrounding the tracked particles, experience pronounced changes in their physical and biogeochemical environments.

5.1. Water Mass Properties at Different Life Stages

The pathways to and from the central California coast and the associated biogeochemical and physical changes are more accurately quantified by considering the location of all tracked particles at four different moments in time (Figure 10).

One year before being seeded in the euphotic layer along the coastline, the distribution of the particles is strongly dominated by water parcels located around the Southern California Bight. Parcels originating from this area are relatively close to the coast already (<500 km offshore), rather deep (>125m) and characterized by high TIN concentrations. This contrasts with the properties of water parcels originating in the north (> 41°N). Not only are these parcels less numerous, they also tend to be located closer to the surface, and consequently their corresponding TIN content is lower.

Around 90 days before the seeding, all parcels have made their way toward central California, hugging the coastline all the way from regions off northwestern Mexico to regions off Vancouver Island. During this journey, the water parcels have shoaled (median changed from 114 to 83 m), but they still retain their median TIN and TON contents of about 16 and 2.5 mmol N/m³, respectively.

Around the time of seeding, the water parcels experience pronounced changes in their physical and biogeochemical signatures. They upwell into the euphotic zone, where their inorganic nutrients are transformed by biological production into organic matter, increasing that pool more than threefold (Figure 11b).

Ninety days after seeding, the particle density reveals a fast and efficient offshore transport to distances exceeding 1,000 km from the coast. This transport is particularly pronounced off central California and occurs much faster than the onward transport in the 90 days prior to seeding. Physical and biogeochemical properties reflect the changes that have occurred within the coastal environment. Basically, all water parcels have made their way into the euphotic zone (median depth is 31 m) and experienced an almost complete depletion of their TIN content (median value dropped from 15.8 to 0.6 mmol N/m³). They still contain some organic matter (median value 4.6 mmol N/m³), even though this value is considerably smaller than that at the time of seeding when productivity was highest (Figure 11b). On their way offshore, only few water parcels subduct

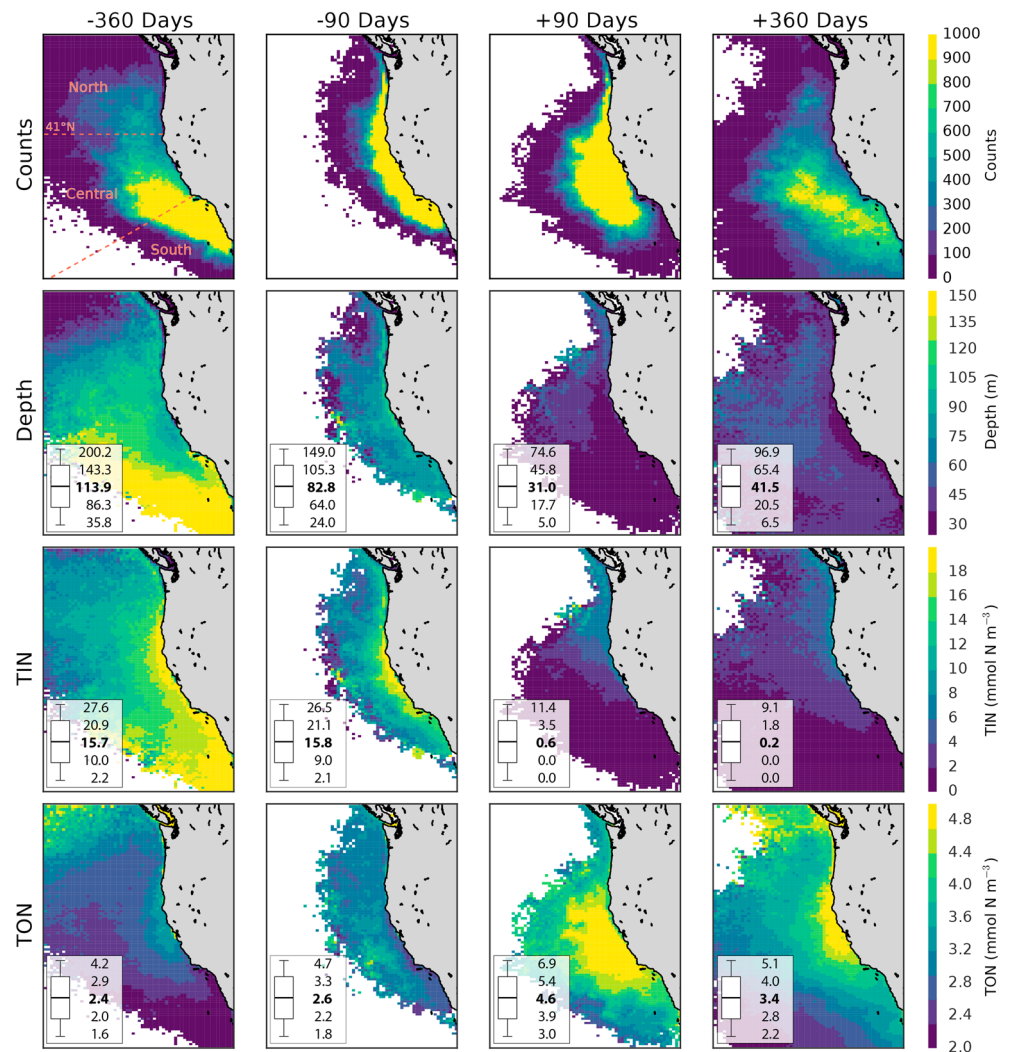


Figure 10. Maps depicting the temporal evolution of all tracked water parcels. The columns show histograms of the different properties at times $t = -360$, $t = -90$, $t = +90$, and $t = +360$ days from their seeding ($t = 0$) in the coastal environment (left to right). Rows depict particle density, depth, total inorganic nitrogen (TIN), and total organic nitrogen (TON; top to bottom). In the bottom left corner of each subplot, the schematic indicates 5th, 25th, 50th (bold), 75th, and 95th percentile values across all trajectories.

deep enough to avoid the surface intensified California Current. Hence, the bulk part of water parcels leaving the coastal upwelling zone is advected southward.

One year past the seeding, the distribution of the tracked particles resembles the initial one in terms of regional predominance, but with an increased offshore and southward displaced and diluted population. From day 90 to day 360 after the upwelling, the particles increased their depth, in particular in the far regions of the central California sector, reflecting the subduction of water parcels as they propagate offshore. The corresponding median TIN value of 0.2 mmol N/m^3 reflects the strong depletion of the inorganic nitrogen for the tracked water parcels at any given location. The water parcels, however, still retain most of their organic matter. Only those trajectories that end up far from the coast have experienced a considerably more pronounced loss of TON.

5.2. Median Evolution of All Trajectories

The median evolution of all 1.4 mio trajectories reveals the characteristic pathways of waters from different regions of origin, their contribution to central California coastal production, and the associated biogeochemical transformations in time (Figure 11).

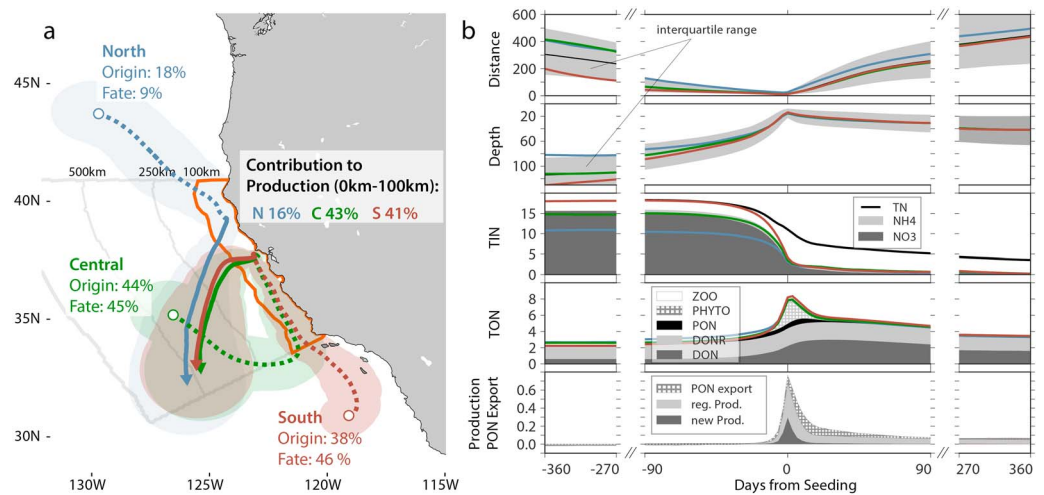


Figure 11. Pathways and biogeochemical evolution of 1.4 mio trajectories during 720 days. (a) Median pathways for particles originating in the north (blue), central (green), and south (red) and their relative contribution to the overall observed production of organic matter along central California. Shaded areas capture 10% of the corresponding trajectory subsample. (b) Median evolution of biogeochemical and physical parameters of all trajectories (black) and those divided into different regions of origin color coded in blue (north), green (central), and red (south). The individual panels depict distance from coast (km), depth (m), contents of TIN (with total nitrogen, TN), TON (and their constituents, in mmol/m^3), and organic matter production and particulate export (in $\text{mmol}\cdot\text{m}^{-3}\cdot\text{day}^{-1}$; from top to bottom). For distance to coast and depth, the gray shading refers to the interquartile range of all trajectories. Note the broken axis in time in order to better illustrate the origin, transformation, and fate of the individual trajectories.

The fraction of trajectories stemming from different latitudinal origins differs strongly. Overall, only 18% of all trajectories originate from latitudes north of Cape Mendocino (41°N). Those particles tend to be advected toward the northern parts of central California, where they get upwelled and subsequently move offshore and southward with the California Current. The 44% that originate from central offshore regions experience a more complex journey. Being initially advected in southeast direction, they feed the coastal poleward flow around Point Conception, get upwelled off central California, and advected offshore, where they eventually join particles originating in the north on their southward journey. The remaining fraction (38%) originates in the Southern California Bight, much closer to the coast than the other populations (see also Chhak & Di Lorenzo, 2007). These particles are transported with the California Undercurrent to the central California coastal region, from where their trajectories follow those of other origins. Thus, while the pathways of different particles toward the central California coast strongly differ from another depending on their origin, those leaving the coastal upwelling zone strongly resemble one another.

Two years after the tracked water parcels started their journey toward the central California upwelling zone, most of them end up in the south (46%), a substantial part is still found in the central sector (45%), while only a very small fraction has traveled up north (9%). The similarity of origin and fate of these trajectories suggests a partial closure of the nutrient cycling in geographical space, with one major restriction: The tracked particles are found in substantially more shallow waters. Having started their journey below the euphotic layer, the majority of the water parcels actually end up within the surface waters. The loop is thus not closed. However, the vertical sinking of particulate matter and its remineralization along the way provides a potential mechanism to close the biogeochemical loop. The corresponding remineralization products replenish the deep inorganic nitrogen pool that gets again advected toward the coastal region and thus facilitates coastal production later on in a *new cycle*.

We estimate the relative contributions of water parcels of a certain region of origin (north, central, and south) to the overall observed production by summing up the nitrogen uptake of all trajectories of a given origin, and comparing it to the overall nitrogen uptake within the coastal upwelling zone. Waters originating in the south contribute 41% to the overall production, those of central and northern origins 43% and 16%, respectively. This differs slightly from the importance by origin (38%, 44%, and 18%, respectively), which is largely a result of the differences in the initial TIN contents.

The temporal evolution further reveals the partitioning of organic matter into the corresponding constituents that are redistributed within the system (Figure 11b). From their initial composition, the water parcels almost triple their TON content around day 0, building up a large pool of phytoplankton biomass. This pool is subsequently routed to different pools of organic matter through zooplankton grazing and the production of both PON and DON. Short-lived pools are eventually routed to DON, which still contains almost double the initial amount of organic matter long after primary production has peaked around day 0. The labile part of DON, which is subject to remineralization, thus potentially fuels regenerated production along the trajectory. This underpins the importance of the dissolved organic pool to fuel offshore regenerated productivity through remnants of remineralization (cf. Letscher et al., 2013).

5.3. Discussion of the Lagrangian Perspective

Only few studies have investigated the origin and fate of water mass trajectories within the CalCS. Two previous contributions addressed this issue using the adjoint of the ROMS tangent linear model (Moore, Arango, et al., 2004) to mainly elucidate nearshore sources of the coastal upwelling and its temporal variability from interannual to decadal time scales and up to 1 month (e.g., Jacox et al., 2015) or 1 year prior to upwelling (e.g., Chhak & Di Lorenzo, 2007). Our results qualitatively agree well with those reported by Chhak and Di Lorenzo (2007) for the central California upwelling region in the sense that they identify the strongest contribution from waters originating in the Southern California Bight at depths of around 150 m. This falls within the depth range that has been reported as the dominant upwelling source between the isopycnals $\sigma_\theta = 25.8 \text{ kg/m}^3$ and $\sigma_\theta = 26.5 \text{ kg/m}^3$ (Bograd et al., 2015). With respect to the latter (which deepens from 200 m in coastal regions to 280 m at 1,000 km offshore in the annual mean), our estimates tend to be somewhat shallower though. However, similar source depths have been identified also in another Lagrangian model study that looked at upwelling source waters along the Oregon coast (Rivas & Samelson, 2011). Their study additionally highlights the importance of alongshore sources to feed the upwelling, though predominantly of northern origin. The agreement of source water depths, and in particular the identification of the importance of alongshore origins is reassuring, considering the overestimation of the nearshore poleward flow in our model (see Figures 4a and 4b). The relative importance of source waters that are located around the Southern California Bight 1 year prior to upwelling thus finds support by previous studies but is likely biased high and hence should be interpreted with caution. On longer time scales of up to 10 years, the relative importance of northern contributions to central California upwelling might strengthen, as salinity and oxygen anomalies on $\sigma_\theta = 26.5 \text{ kg/m}^3$ have been shown to propagate southward from the North Pacific Current into the region of the U.S. West Coast (Poza Buil & Di Lorenzo, 2017). This import of anomalous waters renders the northern branch of the mean gyre circulation an important driver of CalCS decadal biogeochemical variability, but long-term backward integration of upwelling source waters have yet to show such a connection.

To the best of our knowledge, the bias in alongshore circulation is mainly caused by the relatively coarse wind forcing product and the ill-represented wind dropoff (Capet et al., 2004). This has implications for the representation of coastal upwelling (Di Lorenzo, 2003; Song et al., 2011) and production (Renault, Deutsch, et al., 2016) in our model results. A more realistic representation of the coastal wind dropoff would likely lead to a stronger coastal refinement of the upwelling, a deeper upwelling cell, and stronger subduction of water parcels beyond the upwelling front (Song et al., 2011). This might eventually lead to shifts in the regional importance of source water origins. Using a set of idealized wind forcings, for example, Song et al. (2011) identify stronger central and northern entrainment but derive their conclusions from passive tracers that were initiated in July only, when southward flow is at its maximum in the northern CalCS (Hickey, 1979). Our water parcels are initiated whenever the phytoplankton biomass seeding threshold of 10 mmol/m^3 is exceeded (effectively, this is true from March to October). With this substantial difference, we would still expect the associated sources to reveal similar geographical pattern, even with a reduced bias in the alongshore current. These limitations can, however, only be mitigated using dynamically downscaled forcing products or fully coupled model simulations. Addressing this issue will hence be part of future work.

6. Integrating the Eulerian and the Lagrangian Perspectives

By combining the Eulerian and Lagrangian analysis frameworks, we are finally in the position to estimate the fraction of offshore production that is supported by waters exported from the nearshore upwelling region. To this end, we bin all forward trajectories leaving the coastal environment into volumes of 6-km \times 6-km horizontal and 10-m vertical extent within the top 100 m of the water column. This choice is based on an estimate

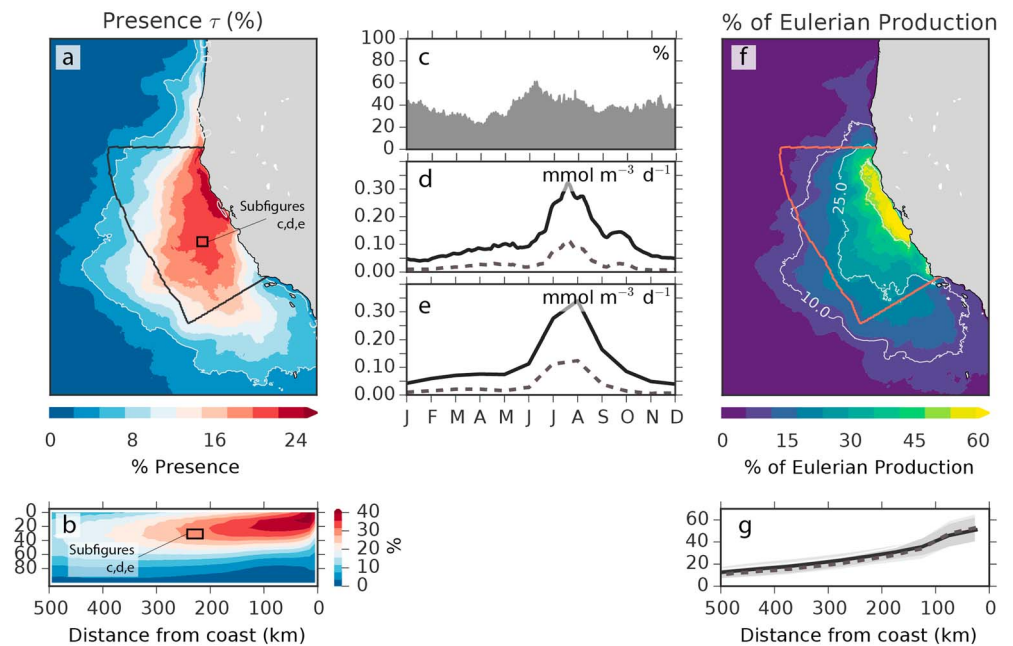


Figure 12. Coastal waters supporting offshore production. (a) Time mean fractional presence τ of coastically originating water parcels averaged within the top 100 m. (b) Vertical cross section of τ computed across the region indicated in (a). (c) Temporal evolution of τ within the square highlighted in (a) and (b) and the corresponding (c) Lagrangian and (d) Eulerian estimates of total (solid) and new (dashed) production throughout the course of the year. (f) Estimated fraction of total production supported by coastal water and (g) its cross-shore profile (dashed line for supported new production; shading represents spatial standard deviation).

of the average volume associated with the particles at the time of seeding. We subsequently compute a fractional presence (τ) of coastal water parcels in each bin for each day of the year (Figures 12a–12c). Within each bin, we also compute the mean nitrogen uptake rates for all the water parcels passing through at a given day (Figure 12d). Finally, we estimate the coastally supported productivity by multiplying the fractional presence (τ) with the mean production rates and comparing these numbers to the Eulerian values.

Integrating the results over the top 100 m clearly reveals the imprint of coastal waters on the offshore environment within the CalCS, reflecting the major transport pathways in offshore and southward direction (Figure 12f). Coastal waters contribute up to 24% to downstream productivity at distances of 500 km. Associated with the main flow of the California Current, the coastal imprint still adds up to more than 10% of the observed production even 750 km from the coast off Southern California and, in some places, extends up to 1,000 km offshore. Further offshore, the coastal influence vanishes. On average, the coastal support amounts to 20% and 13% at distances of 350 and 500 km from the coast, respectively (Figure 12g). Most of the offshore productivity occurs in the form of regenerated production, fueled by the recycling of organic matter initially produced in the nearshore areas. But a considerable part of the production supported by coastal water that occurs through the uptake of coastally derived nitrate is NP. This largely reflects the incomplete assimilation of nitrate within the coastal environment and underpins the importance of the leakage of inorganic nutrients for offshore production (Figure 8c).

Our approach to estimate the fractional contribution of coastally derived nutrients supporting the offshore productivity comes with several limitations. First, our estimate is based on a qualitative seeding approach that does not provide us with accurate volume estimates of each water parcel to assess the production taking place within it. We expect the impact of this caveat to be relatively limited, since we are considering a very large number of particles. Related to our qualitative seeding approach is the uncertainty associated with the binning of water parcels. This turns out to be a more important source of uncertainty. Varying the horizontal bin size between for example, 4 and 10 km changes the estimated contribution of coastal waters to offshore production to values between 7% and 27% at 500-km distance, respectively. This proportional sensitivity is the result of a volumetric change directly affecting the fractional presence (τ) of coastal water parcels in a given offshore environment. While our choice of 6 km \times 6 km is a rather certain estimate of the mean volume, it does

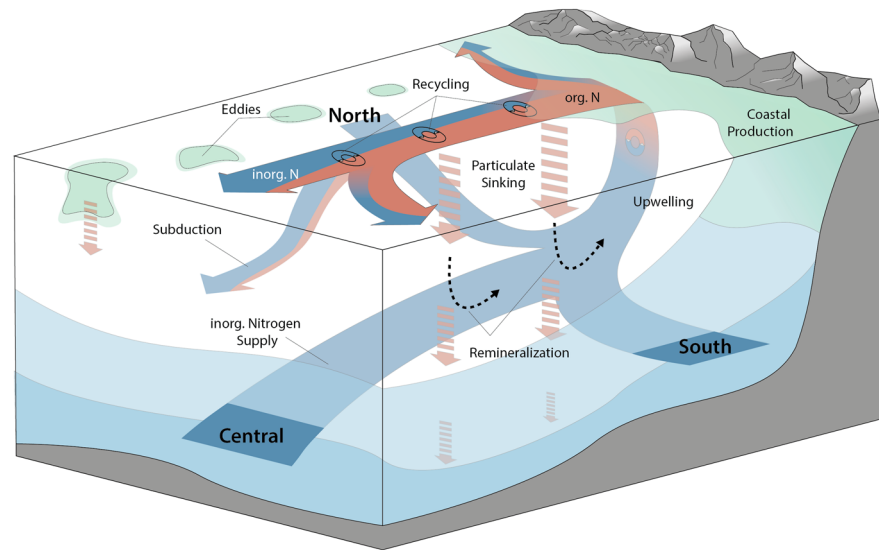


Figure 13. Schematic representation of the three-dimensional biological pump in the California Current System. Nutrient-rich water masses supporting coastal production are imported over long distances and originate from a wide range in geographical space. Subsequent to coastal production, organic matter is laterally displaced, gets recycled along the way, and sinks to deeper layers where remineralization processes feed the reservoir of inorganic constituents. Nutrients supplied to the euphotic zone in the coastal regions are not completely assimilated to organic matter but partly transported into offshore regions. Both organic and inorganic offshore transports support the downstream ecosystem in open ocean environments.

not take into consideration the potential for a correlation between the effective volume of offshore transport and the associated offshore productivity. The determination of this correlation is beyond the scope of this study, but it seems unlikely that this consideration will push the fraction beyond the range considered above. In comparison, we consider the third caveat, that is, the sensitivity of our results to the seeding threshold, as less critical. This is because any change in the threshold tends to lead to a compensating change between the fractional presence and the level of the productivity in the tracked particles. In summary, while our estimates are somewhat uncertain, the conclusions remain firm, that is, waters derived from the nearshore upwelling region fuel a very substantial fraction of the offshore production. Integrated over the 100 to 1,000 km offshore range, this fraction amounts to 16%.

7. Summary and Conclusions

The biological pump in the CalCS is fully three-dimensional. A typical inorganic nutrient molecule that fuels new production within the first 100 km off the coast of central California originates from far away regions, and the resulting organic matter is exported to depth again at great distance from where it was produced (Figure 13). Thus, the equivalence of NP, NCP, and EP that has guided much of the conceptual thinking about the functioning of the biological pump is not applicable in this region (Figure 8; Olivieri & Chavez, 2000; Plattner et al., 2005; Stukel et al., 2011). The same applies most likely for any other EBUS, where the dynamics of ocean circulation is similarly characterized by strong onshore and offshore flows that decouple these productions.

Our model simulations suggest that 70% of the nutrients that support high levels of productivity along central California have been advected over distances of more than 1,000 km during the year prior to their arrival in the coastal upwelling zone. Most of the upwelled nutrients originate from central offshore (44%) and southern alongshore (38%) locations and subsequently contribute to the total production observed along the coastline with similar magnitudes. The strong contribution of nutrients from southern origins emphasizes the relevance of the California Undercurrent in maintaining central California upwelling and hence coastal productivity.

Subsequent to its formation, approximately 36% of the organic matter produced within the first 100 km from the coast is laterally exported to the open ocean. The strongest contribution to this offshore transport comes from dissolved organic matter and this fraction increases from 66% to 93% of the total organic matter flux at 100- and 750-km distance from the coast, respectively. Concurrent with the offshore transport of organic

matter, similar amounts of inorganic nitrogen are laterally exported as well. These nutrients originate from depth as well, but owing to incomplete utilization within the nearshore regions are laterally exported alongside the organic matter.

The lateral export of both inorganic and organic nutrients has strong implications for open ocean productivity. We estimate that 16% of the open ocean production (and subsequently vertical export) within the region between 100 and 1,000 km from the coast is supported by water masses that upwelled along the California coast. This highlights that the influence of coastal processes extends far into the adjacent subtropical gyres (cf. Lovecchio et al., 2017). The majority of this production is fueled by nutrients that are remineralized from the organic matter that has been exported from the nearshore region, illustrating the constant reprocessing of organic matter along the path from the nearshore to the open ocean. The remaining, but still very substantial fraction, is fueled by the laterally exported nitrate, leading to high levels of new production in the offshore regions that also supports elevated levels of export there.

Currently, we cannot quantify well the uncertainties associated with our quantification of the three-dimensional biological pump in the CalCS. Clearly, the results depend on the fidelity of the modeled circulation and the biogeochemical transformation processes. While our evaluation revealed an overall high quality of our modeling system with respect to reproducing key circulation and biogeochemical features, it also revealed a few shortcomings. The most important one is the overly strong northward flowing undercurrent, which likely leads to a moderate overestimation of the contribution of waters of southern origin. We expect the sensitivity to the representation of the biogeochemical processes in the model to be relatively modest, as earlier simulations with substantially higher productivity revealed very similar results (not shown). In fact, all estimates of regional contributions and open ocean supported production changed by maximum 5%. Thus, while the details of our results are likely sensitive to the uncertainties and biases in our modeling system, we consider the overarching conclusions as robust vis-a-vis these uncertainties and biases.

While we were able to disentangle the origin, transformation, and fate of the nutrients along the upper branch of the three-dimensional biological pump in the CalCS, the question remains how the lower branch is closed. A fraction is certainly recycled through a narrow *trapping* loop in which the exported nutrients are remineralized back into the waters that later upwell. This pathway is supported by the fact that even though the origin and fate of the nutrients are far away from where the organic matter is formed, the regions of origin and fate in the CalCS overlap. The remaining fraction must, however, take a much more complex path that may even include a global-scale path through Southern Ocean upwelling and reinjection into mode and intermediate waters (Holzer & Primeau, 2008; Sarmiento et al., 2004). Deciphering this closure of the three-dimensional biological pump remains an intriguing problem to be addressed in future work.

Acknowledgments

We would like to thank Elisa Lovecchio for the fruitful discussions on an early version of the manuscript and Damian Loher for his technical support. We are indebted to Nicolas Grima and Bruno Blanke, who provided technical support to run ARIANE. We thank Emanuele Di Lorenzo and a second reviewer for their thorough work that greatly helped to improve upon the initially submitted manuscript. This research was supported by the Swiss National Science Foundation (Project CALNEX, Grant 149384) and by the Swiss Federal Institute of Technology Zürich (ETH Zürich). Model output data are available online (<https://doi.org/10.3929/ethz-b-000239553>) and may alternatively be obtained upon request (martin.frischknecht@usys.ethz.ch).

References

- Armstrong, R. A., Lee, C., Hedges, J. I., Honjo, S., & Wakeham, S. G. (2002). A new, mechanistic model for organic carbon fluxes in the ocean based on the quantitative association of POC with ballast minerals. *Deep-Sea Research Part II: Topical Studies in Oceanography*, 49(1-3), 219–236. [https://doi.org/10.1016/S0967-0645\(01\)00101-1](https://doi.org/10.1016/S0967-0645(01)00101-1)
- Barth, J. A., Cowles, T. J., Kosro, P. M., Shearman, R. K., Huyer, A., & Smith, R. L. (2002). Injection of carbon from the shelf to offshore beneath the euphotic zone in the California Current. *Journal of Geophysical Research*, 107(C6), 3057. <https://doi.org/10.1029/2001JC000956>
- Barth, J. A., Pierce, S. D., & Cowles, T. J. (2005). Mesoscale structure and its seasonal evolution in the Northern California Current System. *Deep Sea Research Part II: Topical Studies in Oceanography*, 52(1-2), 5–28. <https://doi.org/10.1016/j.dsr2.2004.09.026>
- Barth, J. A., Pierce, S. D., & Smith, R. L. (2000). A separating coastal upwelling jet at Cape Blanco, Oregon and its connection to the California Current System. *Deep Sea Research Part II: Topical Studies in Oceanography*, 47(5-6), 783–810. [https://doi.org/10.1016/S0967-0645\(99\)00127-7](https://doi.org/10.1016/S0967-0645(99)00127-7)
- Bauer, J. E., & Druffel, E. R. (1998). Ocean margins as a significant source of organic matter to the deep open ocean. *Nature*, 392(6675), 482–485. <https://doi.org/10.1038/33122>
- Behrenfeld, M. J., & Falkowski, P. G. (1997). Photosynthetic rates derived from satellite-based chlorophyll concentration. *Limnology and Oceanography*, 42(1), 1–20. <https://doi.org/10.4319/lo.1997.42.1.0001>
- Berelson, W. M., & Stott, L. D. (2003). Productivity and organic carbon rain to the California margin seafloor: Modern and paleoceanographic perspectives. *Paleoceanography*, 18(1), 1002. <https://doi.org/10.1029/2001PA000672>
- Berger, W. H. (1989). Global maps of ocean productivity. In W. H. Berger, V. S. Smetacek, & G. Wefer (Eds.), *Productivity of the ocean: Present and past* (pp. 429–456). New York: J. Wiley and Sons.
- Beusen, A. H. W. (2014). Transport of nutrients from land to sea: Global modeling approaches and uncertainty analyses (Ph.D. thesis), Utrecht University. <https://dspace.library.uu.nl/handle/1874/298665>
- Biscaye, P. E., Flagg, C. N., & Falkowski, P. G. (1994). The shelf edge exchange processes experiment, SEEP-II: An introduction to hypotheses, results and conclusions. *Deep Sea Research Part II: Topical Studies in Oceanography*, 41(2-3), 231–252. [https://doi.org/10.1016/0967-0645\(94\)90022-1](https://doi.org/10.1016/0967-0645(94)90022-1)
- Blanke, B., & Raynaud, S. (1997). Kinematics of the Pacific equatorial undercurrent: An Eulerian and Lagrangian approach from GCM results. *Journal of Physical Oceanography*, 27(6), 1038–1053. [https://doi.org/10.1175/1520-0485\(1997\)0272.0.CO;2](https://doi.org/10.1175/1520-0485(1997)0272.0.CO;2)

- Bograd, S. J., Buil, M. P., Lorenzo, E. D., Castro, C. G., Schroeder, I. D., Goericke, R., et al. (2015). Changes in source waters to the Southern California Bight. *Deep Sea Research Part II: Topical Studies in Oceanography*, 112, 42–52. <https://doi.org/10.1016/j.dsr2.2014.04.009>
- Brink, K. H., & Cowles, T. J. (1991). The Coastal Transition Zone program. *Journal of Geophysical Research*, 96(C8), 14,637. <https://doi.org/10.1029/91JC01206>
- Brodeau, L., Barnier, B., Treguier, A. M., Penduff, T., & Gulev, S. (2010). An ERA40-based atmospheric forcing for global ocean circulation models. *Ocean Modelling*, 31(3-4), 88–104. <https://doi.org/10.1016/j.ocemod.2009.10.005>
- Buesseler, K. O., Antia, A. N., Chen, M., Fowler, S. W., Gardner, W. D., Gustafsson, O., et al. (2007). An assessment of the use of sediment traps for estimating upper ocean particle fluxes. *Journal of Marine Research*, 65(3), 345–416. <https://doi.org/10.1357/002224007781567621>
- Buesseler, K. O., Lamborg, C. H., Boyd, P. W., Lam, P. J., Trull, T. W., Bidigare, R. R., et al. (2007). Revisiting carbon flux through the ocean's twilight zone. *Science*, 316(5824), 567–570. <https://doi.org/10.1126/science.1137959>
- Capet, X. J., Marchesiello, P., & McWilliams, J. C. (2004). Upwelling response to coastal wind profiles. *Geophysical Research Letters*, 31, L13311. <https://doi.org/10.1029/2004GL020123>
- Carpenter, R. L., Droegemeier, K. K., Woodward, P. R., & Hane, C. E. (1990). Application of the piecewise parabolic method (PPM) to meteorological modeling. *Monthly Weather Review*, 118(3), 586–612. [https://doi.org/10.1175/1520-0493\(1990\)118<0586:AOTPPM>2.0.CO;2](https://doi.org/10.1175/1520-0493(1990)118<0586:AOTPPM>2.0.CO;2)
- Carton, J. A., & Giese, B. S. (2008). A reanalysis of ocean climate using Simple Ocean Data Assimilation (SODA). *Monthly Weather Review*, 136(8), 2999–3017. <https://doi.org/10.1175/2007MWR1978.1>
- Chhak, K., & Di Lorenzo, E. (2007). Decadal variations in the California Current upwelling cells. *Geophysical Research Letters*, 34, L14,604. <https://doi.org/10.1029/2007GL030203>
- Colella, P., & Woodward, P. R. (1984). The piecewise parabolic method (PPM) for gas-dynamical simulations. *Journal of Computational Physics*, 54(1), 174–201. [https://doi.org/10.1016/0021-9991\(84\)90143-8](https://doi.org/10.1016/0021-9991(84)90143-8)
- Combes, V., Chenillat, F., Di Lorenzo, E., Rivière, P., Ohman, M., & Bograd, S. (2013). Cross-shore transport variability in the California Current: Ekman upwelling vs. eddy dynamics. *Progress in Oceanography*, 109, 78–89. <https://doi.org/10.1016/j.pocean.2012.10.001>
- Dai, A., Qian, T., Trenberth, K. E., & Milliman, J. D. (2009). Changes in continental freshwater discharge from 1948 to 2004. *Journal of Climate*, 22(10), 2773–2792. <https://doi.org/10.1175/2008JCLI2592.1>
- Dale, A. W., Nickelsen, L., Scholz, F., Hensen, C., Oschlies, A., & Wallmann, K. (2015). A revised global estimate of dissolved iron fluxes from marine sediments. *Global Biogeochemical Cycles*, 29, 691–707. <https://doi.org/10.1002/2014GB005017>
- Davis, A., Di Lorenzo, E., Luo, H., Belmadani, A., Maximenko, N., Melnichenko, O., et al. (2014). Mechanisms for the emergence of ocean striations in the North Pacific. *Geophysical Research Letters*, 41, 948–953. <https://doi.org/10.1002/2013GL057956>
- DeVries, T., & Weber, T. (2017). The export and fate of organic matter in the ocean: New constraints from combining satellite and oceanographic tracer observations. *Global Biogeochemical Cycles*, 31, 535–555. <https://doi.org/10.1002/2016GB005551>
- Dee, D. P., Uppala, S. M., Simmons, A. J., Berrisford, P., Poli, P., Kobayashi, S., et al. (2011). The ERA-Interim reanalysis: Configuration and performance of the data assimilation system. *Quarterly Journal of the Royal Meteorological Society*, 137(656), 553–597. <https://doi.org/10.1002/qj.828>
- Devol, A. H., & Hartnett, H. E. (2001). Role of the oxygen-deficient zone in transfer of organic carbon to the deep ocean. *Limnology and Oceanography*, 46(7), 1684–1690. <https://doi.org/10.4319/lo.2001.46.7.1684>
- Di Lorenzo, E. (2003). Seasonal dynamics of the surface circulation in the Southern California Current System. *Deep Sea Research Part II: Topical Studies in Oceanography*, 50(14-16), 2371–2388. [https://doi.org/10.1016/S0967-0645\(03\)00125-5](https://doi.org/10.1016/S0967-0645(03)00125-5)
- Ducklow, H., & McCallister, J. L. (2004). The biogeochemistry of carbon dioxide in the coastal oceans. In A. Robinson & K. Brink (Eds.), *The sea, volume 13: The global coastal ocean: Multiscale interdisciplinary processes* (pp. 269–315). Global Change-The IGBP Series. Cambridge, Mass: Harvard Univ. Press.
- Ducklow, H., Steinberg, D., & Buesseler, K. (2001). Upper ocean carbon export and the biological pump. *Oceanography*, 14(4), 50–58. <https://doi.org/10.5670/oceanog.2001.06>
- Dugdale, R. C., & Goering, J. J. (1967). Uptake of new and regenerated forms of nitrogen in primary productivity. *Limnology and Oceanography*, 12(2), 196–206. <https://doi.org/10.4319/lo.1967.12.2.0196>
- Dunne, J. P., Armstrong, R. A., Gnanadesikan, A., & Sarmiento, J. L. (2005). Empirical and mechanistic models for the particle export ratio. *Global Biogeochemical Cycles*, 19, GB4026. <https://doi.org/10.1029/2004GB002390>
- Dunne, J. P., Sarmiento, J. L., & Gnanadesikan, A. (2007). A synthesis of global particle export from the surface ocean and cycling through the ocean interior and on the seafloor. *Global Biogeochemical Cycles*, 21, GB4006. <https://doi.org/10.1029/2006GB002907>
- Dussin, R., Barnier, B., & Brodeau, L., & Molines, J. M. (2016). The making of Drakkar forcing set DF55 (*Tech. rep. 01-04-16*). Grenoble, France: LGGE. <https://www.drakkar-ocean.eu/publications/reports>
- Eppley, R. W., & Peterson, B. J. (1979). Particulate organic matter flux and planktonic new production in the deep ocean. *Nature*, 282(5740), 677–680. <https://doi.org/10.1038/282677a0>
- Friskhnecht, M., Münnich, M., & Gruber, N. (2015). Remote versus local influence of ENSO on the California Current System. *Journal of Geophysical Research: Oceans*, 120, 1353–1374. <https://doi.org/10.1002/2014JC010531>
- Friskhnecht, M., Münnich, M., & Gruber, N. (2017). Local atmospheric forcing driving an unexpected California Current System response during the 2015–2016 El Niño. *Geophysical Research Letters*, 44, 304–311. <https://doi.org/10.1002/2016GL071316>
- García, H., Locarnini, R., Boyer, T., Antonov, J., Baranova, O., Zweng, M., et al. (2013a). World ocean atlas 2013, Volume 3: Dissolved oxygen, apparent oxygen utilization, and oxygen saturation. In S. Levitus & A. Mishonov (Eds.), NOAA Atlas NESDIS 75, pp. 27. Silver Springs, MD.
- García, H., Locarnini, R., Boyer, T., Antonov, J., Baranova, O., Zweng, M., et al. (2013b). World OCEAN ATLAS 2013, Volume 4: Dissolved inorganic nutrients (phosphate, nitrate, silicate). In S. Levitus & A. Mishonov (Eds.), NOAA Atlas NESDIS 75, pp. 27. Silver Springs, MD.
- García-Muñoz, M., Aristegui, J., Pelegrí, J. L., Antoranz, A., Ojeda, A., & Torres, M. (2005). Exchange of carbon by an upwelling filament off Cape Ghir (NW Africa). *Journal of Marine Systems*, 54(1-4), 83–95. <https://doi.org/10.1016/j.jmarsys.2004.07.005>
- Gent, P. R., Danabasoglu, G., Donner, L. J., Holland, M. M., Hunke, E. C., Jayne, S. R., et al. (2011). The Community Climate System Model version 4. *Journal of Climate*, 24(19), 4973–4991. <https://doi.org/10.1175/2011JCLI4083.1>
- Gruber, N., Frenzel, H., Doney, S. C., Marchesiello, P., McWilliams, J. C., Moisan, J. R., et al. (2006). Eddy-resolving simulation of plankton ecosystem dynamics in the California Current System. *Deep Sea Research Part I: Oceanographic Research Papers*, 53(9), 1483–1516. <https://doi.org/10.1016/j.dsr.2006.06.005>
- Gruber, N., Lachkar, Z., Frenzel, H., Marchesiello, P., Münnich, M., McWilliams, J. C., et al. (2011). Eddy-induced reduction of biological production in eastern boundary upwelling systems. *Nature Geoscience*, 4(11), 787–792. <https://doi.org/10.1038/ngeo1273>
- Hales, B., Karp-Boss, L., Perlin, A., & Wheeler, P. A. (2006). Oxygen production and carbon sequestration in an upwelling coastal margin. *Global Biogeochemical Cycles*, 20, GB3001. <https://doi.org/10.1029/2005GB002517>
- Hansell, D., Carlson, C., Repeta, D., & Schlitzer, R. (2009). Dissolved organic matter in the ocean: A controversy stimulates new insights. *Oceanography*, 22(4), 202–211. <https://doi.org/10.5670/oceanog.2009.109>

- Haumann, A. (2016). Southern ocean response to recent changes in surface freshwater fluxes (Ph.D. thesis), ETH Zurich. <https://doi.org/10.3929/ethz-b-000166276>
- Henson, S. A., Sanders, R., Madsen, E., Morris, P. J., Le Moigne, F., & Quartly, G. D. (2011). A reduced estimate of the strength of the ocean's biological carbon pump. *Geophysical Research Letters*, *38*, L04,606. <https://doi.org/10.1029/2011GL046735>
- Hickey, B. M. (1979). The California Current System—Hypotheses and facts. *Progress in Oceanography*, *8*(4), 191–279.
- Holzer, M., & Primeau, F. W. (2008). The path-density distribution of oceanic surface-to-surface transport. *Journal of Geophysical Research*, *113*, C01,018. <https://doi.org/10.1029/2006JC003976>
- Honjo, S., Dymond, J., Collier, R., & Manganini, S. J. (1995). Export production of particles to the interior of the equatorial Pacific Ocean during the 1992 EqPac experiment. *Deep-Sea Research Part II*, *42*(2-3), 831–870. [https://doi.org/10.1016/0967-0645\(95\)00034-N](https://doi.org/10.1016/0967-0645(95)00034-N)
- Jacox, M. G., Fiechter, J., Moore, A. M., & Edwards, C. A. (2015). ENSO and the California Current coastal upwelling response. *Journal of Geophysical Research C: Oceans*, *120*, 1691–1702. <https://doi.org/10.1002/2014JC010650>
- Jahnke, R. A. (1990). Early diagenesis and recycling of biogenic debris at the seafloor, Santa Monica Basin, California. *Journal of Marine Research*, *48*(2), 413–436. <https://doi.org/10.1357/002224090784988773>
- Kahru, M., Kudela, R., Manzano-Sarabia, M., & Mitchell, B. G. (2009). Trends in primary production in the California Current detected with satellite data. *Journal of Geophysical Research*, *114*, C02,004. <https://doi.org/10.1029/2008JC004979>
- Knauer, G. A., Karl, D. M., Martin, J. H., & Hunter, C. N. (1984). In situ effects of selected preservatives on total carbon, nitrogen and metals collected in sediment traps. *Journal of Marine Research*, *42*(2), 445–462. <https://doi.org/10.1357/002224084788502710>
- Krause, J. W., Brzezinski, M. A., Goericke, R., Landry, M. R., Ohman, M. D., Stukel, M. R., & Taylor, A. G. (2015). Variability in diatom contributions to biomass, organic matter production and export across a frontal gradient in the California Current ecosystem. *Journal of Geophysical Research: Oceans*, *120*, 1032–1047. <https://doi.org/10.1002/2014JC010472>
- Lachkar, Z., & Gruber, N. (2011). What controls biological production in coastal upwelling systems? Insights from a comparative modeling study. *Biogeosciences*, *8*(10), 2961–2976. <https://doi.org/10.5194/bg-8-2961-2011>
- Lamarque, J. F., Dentener, F., McConnell, J., Ro, C. U., Shaw, M., Vet, R., et al. (2013). Multi-model mean nitrogen and sulfur deposition from the atmospheric chemistry and climate model intercomparison project (ACCMIP): Evaluation of historical and projected future changes. *Atmospheric Chemistry and Physics*, *13*(16), 7997–8018. <https://doi.org/10.5194/acp-13-7997-2013>
- Large, W. G., McWilliams, J. C., & Doney, S. C. (1994). Oceanic vertical mixing: A review and a model with a nonlocal boundary layer parameterization. *Reviews of Geophysics*, *32*(4), 363. <https://doi.org/10.1029/94RG01872>
- Large, W. G., & Yeager, S. G. (2009). The global climatology of an interannually varying air-sea flux data set. *Climate Dynamics*, *33*(2-3), 341–364. <https://doi.org/10.1007/s00382-008-0441-3>
- Laufkötter, C., John, J. G., Stock, C. A., & Dunne, J. P. (2017). Temperature and oxygen dependence of the remineralization of organic matter. *Global Biogeochemical Cycles*, *31*, 1038–1050. <https://doi.org/10.1002/2017GB005643>
- Laws, E. A., Falkowski, P. G., Smith, W. O., Ducklow, H., & McCarthy, J. J. (2000). Temperature effects on export production in the open ocean. *Global Biogeochemical Cycles*, *14*(4), 1231–1246. <https://doi.org/10.1029/1999GB001229>
- Letscher, R. T., Hansell, D. A., Carlson, C. A., Lumpkin, R., & Knapp, A. N. (2013). Dissolved organic nitrogen in the global surface ocean: Distribution and fate. *Global Biogeochemical Cycles*, *27*, 141–153. <https://doi.org/10.1029/2012GB004449>
- Levitus, S., Boyer, T. P., Garcia, H. E., Locarnini, R. A., Zweng, M. M., Mishonov, A. V., et al. (2014). World ocean atlas 2013 (NCEI Accession 0114815). vol. Version 3., National Oceanographic Data Center, NOAA. <https://doi.org/10.7289/V5F769GT>
- Lévy, M., Bopp, L., Karleskind, P., Resplandy, L., Ethe, C., & Pinsard, F. (2013). Physical pathways for carbon transfers between the surface mixed layer and the ocean interior. *Global Biogeochemical Cycles*, *27*, 1001–1012. <https://doi.org/10.1002/gbc.20092>
- Lévy, M., Ferrari, R., Franks, P. J., Martin, A. P., & Rivière, P. (2012). Bringing physics to life at the submesoscale. *Geophysical Research Letters*, *39*, L14,602. <https://doi.org/10.1029/2012GL052756>
- Lima, I. D., Lam, P. J., & Doney, S. C. (2014). Dynamics of particulate organic carbon flux in a global ocean model. *Biogeosciences*, *11*(4), 1177–1198. <https://doi.org/10.5194/bg-11-1177-2014>
- Liu, K.-K., Atkinson, L., Quiñones, R. A., & Talaue-McManus, L. (2010). Biogeochemistry of continental margins in a global context. In K.-K. Liu, L. Atkinson, R. Quiñones, & L. Talaue-McManus (Eds.), *Global Change-The IGBP Series* pp. 3–24. Berlin, Heidelberg: Springer. https://doi.org/10.1007/978-3-540-92735-8_1
- Lovecchio, E., Gruber, N., & Münnich, M. (2018). Mesoscale contribution to the long-range offshore transport of organic carbon from the Canary upwelling system to the open North Atlantic. *Biogeosciences*, *15*, 5061–5091. <https://doi.org/10.5194/bg-15-5061-2018>
- Lovecchio, E., Gruber, N., Münnich, M., & Lachkar, Z. (2017). On the long-range offshore transport of organic carbon from the Canary upwelling system to the open North Atlantic. *Biogeosciences*, *14*(13), 3337–3369. <https://doi.org/10.5194/bg-14-3337-2017>
- Marchesiello, P., McWilliams, J., & Shchepetkin, A. (2003). Equilibrium structure and dynamics of the California Current System. *Journal of Physical Oceanography*, *33*(4), 753–783. [https://doi.org/10.1175/1520-0485\(2003\)332.0.CO;2](https://doi.org/10.1175/1520-0485(2003)332.0.CO;2)
- Martin, J. H., Knauer, G. A., Karl, D. M., & Broenkow, W. W. (1987). VERTEx: carbon cycling in the northeast Pacific. *Deep Sea Research Part A, Oceanographic Research Papers*, *34*(2), 267–285. [https://doi.org/10.1016/0198-0149\(87\)90086-0](https://doi.org/10.1016/0198-0149(87)90086-0)
- McGillicuddy, D. J. (2016). Mechanisms of physical-biological-biogeochemical interaction at the oceanic mesoscale. *Annual Review of Marine Science*, *8*(1), 125–159. <https://doi.org/10.1146/annurev-marine-010814-015606>
- Moore, A. M., Arango, H. G., Di Lorenzo, E., Cornuelle, B. D., Miller, A. J., & Neilson, D. J. (2004). A comprehensive ocean prediction and analysis system based on the tangent linear and adjoint of a regional ocean model. *Ocean Modelling*, *7*(1-2), 227–258. <https://doi.org/10.1016/j.ocemod.2003.11.001>
- Moore, J. K., & Braucher, O. (2008). Sedimentary and mineral dust sources of dissolved iron to the world ocean. *Biogeosciences*, *5*(3), 631–656. <https://doi.org/10.5194/bg-5-631-2008>
- Moore, J. K., Doney, S. C., & Lindsay, K. (2004). Upper ocean ecosystem dynamics and iron cycling in a global three-dimensional model. *Global Biogeochemical Cycles*, *18*, GB4028. <https://doi.org/10.1029/2004GB002220>
- Moore, J. K., Lindsay, K., Doney, S. C., Long, M. C., & Misumi, K. (2013). Marine ecosystem dynamics and biogeochemical cycling in the community earth system model [CESM1(BGC)]: Comparison of the 1990s with the 2090s under the RCP4.5 and RCP8.5 Scenarios. *Journal of Climate*, *26*(23), 9291–9312. <https://doi.org/10.1175/JCLI-D-12-00566.1>
- Morel, A., & Berthon, J.-F. (1989). Surface pigments, algal biomass profiles, and potential production of the euphotic layer: Relationships reinvestigated in view of remote-sensing applications. *Limnology and Oceanography*, *34*(8), 1545–1562. <https://doi.org/10.4319/lo.1989.34.8.1545>
- Munro, D. R., Quay, P. D., Juranek, L. W., & Goericke, R. (2013). Biological production rates off the Southern California coast estimated from triple O₂ isotopes and O₂:Ar gas ratios. *Limnology and Oceanography*, *58*(4), 1312–1328. <https://doi.org/10.4319/lo.2013.58.4.1312>

- Nagai, T., Gruber, N., Frenzel, H., Lachkar, Z., McWilliams, J. C., & Plattner, G.-K. (2015). Dominant role of eddies and filaments in the offshore transport of carbon and nutrients in the California Current System. *Journal of Geophysical Research: Oceans*, *120*, 5318–5341. <https://doi.org/10.1002/2015JC010889>
- Olivieri, R. A., & Chavez, F. P. (2000). A model of plankton dynamics for the coastal upwelling system of Monterey Bay, California. *Deep-Sea Research II*, *47*(5–6), 1077–1106. [https://doi.org/10.1016/S0967-0645\(99\)00137-X](https://doi.org/10.1016/S0967-0645(99)00137-X)
- Omand, M. M., D'Asaro, E. A., Lee, C. M., Perry, M. J., Briggs, N., Cetinić, I., & Mahadevan, A. (2015). Eddy-driven subduction exports particulate organic carbon from the spring bloom. *Science*, *348*(6231), 222–225. <https://doi.org/10.1126/science.1260062>
- Pelegrí, J., Aristegui, J., Cana, L., González-Dávila, M., Hernández-Guerra, A., Hernández-León, S., et al. (2005). Coupling between the open ocean and the coastal upwelling region off northwest Africa: Water recirculation and offshore pumping of organic matter. *Journal of Marine Systems*, *54*(1–4), 3–37. <https://doi.org/10.1016/j.jmarsys.2004.07.003>
- Pennington, J., Gernot, E., Carmen, G., Curt, A., Wiley, W., & Francisco, P. (2010). The Northern and Central California coastal upwelling system. In K.-K. Liu, L. Atkinson, R. Quiñones, & L. Talaeue-McManus (Eds.), *Carbon and nutrient fluxes in continental margins* (pp. 29–44). Global Change The IGBP Series: Berlin. Springer. https://doi.org/10.1007/978-3-540-92735-8_2
- Plattner, G.-K., Gruber, N., Frenzel, H., & McWilliams, J. C. (2005). Decoupling marine export production from new production. *Geophysical Research Letters*, *32*, L11,612. <https://doi.org/10.1029/2005GL022660>
- Pozo Buil, M., & Di Lorenzo, E. (2017). Decadal dynamics and predictability of oxygen and subsurface tracers in the California Current System. *Geophysical Research Letters*, *44*, 4204–4213. <https://doi.org/10.1002/2017GL072931>
- Renault, L., Deutsch, C., McWilliams, J. C., Frenzel, H., Liang, J.-H., & Colas, F. (2016). Partial decoupling of primary productivity from upwelling in the California Current System. *Nature Geoscience*, *9*(7), 505–508. <https://doi.org/10.1038/ngeo2722>
- Renault, L., Hall, A., & McWilliams, J. C. (2016). Orographic shaping of US West Coast wind profiles during the upwelling season. *Climate Dynamics*, *46*(1–2), 273–289. <https://doi.org/10.1007/s00382-015-2583-4>
- Reynolds, R. W., Smith, T. M., Liu, C., Chelton, D. B., Casey, K. S., & Schlax, M. G. (2007). Daily high-resolution-blended analyses for sea surface temperature. *Journal of Climate*, *20*(22), 5473–5496. <https://doi.org/10.1175/2007JCLI1824.1>
- Ridgway, K., Dunn, J., & Wilkin, J. (2002). Ocean interpolation by four-dimensional weighted least squares - application to the waters around Australasia. *Journal of Atmospheric and Oceanic Technology*, *19*(9), 1357–1375. [https://doi.org/10.1175/1520-0426\(2002\)0192.0.CO;2](https://doi.org/10.1175/1520-0426(2002)0192.0.CO;2)
- Rivas, D., & Samelson, R. M. (2011). A numerical modeling study of the upwelling source waters along the Oregon Coast during 2005. *Journal of Physical Oceanography*, *41*(1), 88–112. <https://doi.org/10.1175/2010JPO4327.1>
- Rudnick, D. L., Zaba, K. D., Todd, R. E., & Davis, R. E. (2017). A climatology of the California Current System from a network of underwater gliders. *Progress in Oceanography*, *154*, 64–106. <https://doi.org/10.1016/j.pocean.2017.03.002>
- Scientific Committee of Oceanic Research (1990). The Joint Global Ocean Flux Study (JGOFS) science plan. JGOFS Report, 5(Report No. 5), 1–61.
- Sarmiento, J. L., & Gruber, N. (2006). *Ocean biogeochemical dynamics* (503 pp.). Princeton, NJ: Princeton University Press.
- Sarmiento, J. L., Gruber, N., Brzezinski, M. A., & Dunne, J. P. (2004). High-latitude controls of thermocline nutrients and low latitude biological productivity. *Nature*, *427*(6969), 56–60. <https://doi.org/10.1038/nature02127>
- Schlitzer, R. (2004). Export production in the equatorial and North Pacific derived from dissolved oxygen, nutrient and carbon data. *Journal of Oceanography*, *60*(1), 53–62. <https://doi.org/10.1023/B:JOCE.0000038318.38916.e6>
- Shchepetkin, A. F., & McWilliams, J. C. (2005). The Regional Oceanic Modeling System (ROMS): A split-explicit, free-surface, topography-following-coordinate oceanic model. *Ocean Modelling*, *9*(4), 347–404. <https://doi.org/10.1016/j.ocemod.2004.08.002>
- Siegel, D. A., Buesseler, K. O., Doney, S. C., Saille, S. F., Behrenfeld, M. J., & Boyd, P. W. (2014). Global assessment of ocean carbon export by combining satellite observations and food-web models. *Global Biogeochemical Cycles*, *28*, 181–196. <https://doi.org/10.1002/2013GB004743>
- Siegel, D. A., Fields, E., & Buesseler, K. O. (2008). A bottom-up view of the biological pump: Modeling source funnels above ocean sediment traps. *Deep-Sea Research Part I: Oceanographic Research Papers*, *55*(1), 108–127. <https://doi.org/10.1016/j.dsr.2007.10.006>
- Smith, P. E., & Eppley, R. W. (1982). Primary production and the anchovy population in the Southern California Bight: Comparison of time series. *Limnology and Oceanography*, *27*(1), 1–17. <https://doi.org/10.4319/lo.1982.27.1.0001>
- Song, H., Miller, A. J., Cornuelle, B. D., & Di Lorenzo, E. (2011). Changes in upwelling and its water sources in the California Current System driven by different wind forcing. *Dynamics of Atmospheres and Oceans*, *52*(1–2), 170–191. <https://doi.org/10.1016/j.dynatmoce.2011.03.001>
- Stukel, M. R., Aluwihare, L. I., Barbeau, K. A., Chekalyuk, A. M., Goericke, R., Miller, A. J., et al. (2017). Mesoscale ocean fronts enhance carbon export due to gravitational sinking and subduction. *PNAS*, *114*(6), 1252–1257. <https://doi.org/10.1073/pnas.1609435114>
- Stukel, M. R., Landry, M. R., Benitez-Nelson, C. R., & Goericke, R. (2011). Trophic cycling and carbon export relationships in the California Current ecosystem. *Limnology and Oceanography*, *56*(5), 1866–1878. <https://doi.org/10.4319/lo.2011.56.5.1866>
- Taylor, K. E. (2001). Summarizing multiple aspects of model performance in a single diagram. *Journal of Geophysical Research*, *106*(D7), 7183. <https://doi.org/10.1029/2000JD900719>
- Thomas, H., Bozec, Y., Elkalay, K., & De Baar, H. J. (2004). Enhanced open ocean storage of CO₂ from shelf sea pumping. *Science*, *304*(5673), 1005–1008. <https://doi.org/10.1126/science.1095491>
- Walsh, J. J. (1991). Importance of continental margins in the marine biogeochemical cycling of carbon and nitrogen. *Nature*, *350*(6313), 53–55. <https://doi.org/10.1038/350053a0>
- Williams, R., & Follows, M. (2003). Physical transport of nutrients and the maintenance of biological production. In M. J. R. Fasham (Ed.), *Ocean biogeochemistry: The role of the ocean carbon cycle in global change* (pp. 19–51), chap. 2. Berlin, Heidelberg: Springer. https://doi.org/10.1007/978-3-642-55844-3_3
- Willmott, C. J. (1981). On the validation of models. *Physical Geography*, *2*(2), 184–194. <https://doi.org/10.1080/02723646.1981.10642213>
- Wong, C., Whitney, F., Crawford, D., Iseki, K., Matear, R., Johnson, W., et al. (1999). Seasonal and interannual variability in particle fluxes of carbon, nitrogen and silicon from time series of sediment traps at Ocean Station P, 1982–1993: relationship to changes in subarctic primary productivity. *Deep Sea Research Part II: Topical Studies in Oceanography*, *46*(11–12), 2735–2760. [https://doi.org/10.1016/S0967-0645\(99\)00082-X](https://doi.org/10.1016/S0967-0645(99)00082-X)
- Yang, S., Gruber, N., Long, M. C., & Vogt, M. (2017). ENSO-driven variability of denitrification and Suboxia in the Eastern tropical Pacific Ocean. *Global Biogeochemical Cycles*, *31*, 1470–1487. <https://doi.org/10.1002/2016GB005596>